Air Products and Chemicals

HOUDRY TECHNICAL CENTER

FE-2033-7
UC-90-C

HOT LOW BTU PRODUCER GAS DESULFURIZATION IN FIXED BED OF IRON OXIDE FLY-ASH

MONTHLY REPORT NO. 6
1 DECEMBER TO 31 DECEMBER 1975

QUARTERLY REPORT NO. 2
1 OCTOBER TO 31 DECEMBER 1975

ERNEST L. LEUENBERGER

AIR PRODUCTS AND CHEMICALS, INC.
HOUDRY TECHNICAL CENTER
P. O. BOX 427
MARCUS HOOK, PENNSYLVANIA 19061

DATE PUBLISHED - 27 FEBRUARY 1976

PREPARED FOR THE UNITED STATES
ENERGY RESEARCH AND DEVELOPMENT ADMINISTRATION

UNDER CONTRACT NO. E (49-18)2033

TABLE OF CONTENTS

TABLE OF CONTENTS (Cont.)

LIST OF TABLES

LIST OF FIGURES

Air Products and Chemicals INC
HOUDRY TECHNICAL CENTER

ERDA CONTRACT E(49-18)2033

AIR PRODUCTS AND CHEMICALS, INC.
MARCUS HOOK, PENNSYLVANIA 19061

MONTHLY REPORT NO. 6, 1 DECEMBER TO 31 DECEMBER 1975

QUARTERLY REPORT NO. 2, 1 OCTOBER TO 31 DECEMBER 1975

ABSTRACT

This is the sixth monthly and second quarterly progress report of the APCI support program to assist ERDA in the development of their hot producer gas desulfurization process. An iron oxide-fly ash absorbent will be used in a cyclic fixed-bed operation. Specific objectives of APCI are absorbent development, definition of process scale-up criteria, and commercial process design.

Major emphasis this period has been in the following areas:

1. Preparation of experimental sorbents

   Physical properties and chemical analyses of prepared sorbents are listed.

2. Dynamic absorption tests of experimental sorbents

   Dynamic testing is explained. Test results for sorbents with different iron oxide sources are presented.

3. Derivation of differential equations to describe sorption dynamics

   The differential equations and derivations for mass and heat transfer are presented. A plan of attack for the solution of these equations is described.

4. Computer programming the isothermal sorption dynamics equations

   The solution to the isothermal sorption equations is presented. Predicted effects of changes in sorption operating conditions and sorbent properties are discussed.

5. Comparison between experimental dynamic tests and computer model predictions

   The isothermal sorption model agrees with experimental data for H_2S sorption on iron oxide/fly ash sorbents. The model is used to correlate dynamic data on sorbents using different iron oxide sources. Acceptable sources of iron oxide are identified.

ERDA CONTRACT E(49-18)2033

The applicability of the work accomplished this quarter on sorber design is demonstrated. The isothermal model is used to prepare a preliminary design of a sorber with a capacity of 120M SCFH process gas. Sorbent properties obtained from dynamic tests are used in the model.

ERDA CONTRACT E(49-18)2033

AIR PRODUCTS AND CHEMICALS, INC.
MARCUS HOOK, PENNSYLVANIA 19061

MONTHLY REPORT NO. 6, 1 DECEMBER TO 31 DECEMBER 1975

QUARTERLY REPORT NO. 2, 1 OCTOBER TO 31 DECEMBER 1975

I. INTRODUCTION

The Air Products and Chemicals, Inc. Research, Development, and Engineering program is aimed at assisting ERDA in developing their hot producer gas desulfurization process. A cyclic fixed-bed technique using an iron oxide-fly ash absorbent at producer gas temperature and pressure is the ultimate objective. The process is being developed by ERDA at the Morgantown Energy Research Center.

Specific objectives of the APCI support program are absorbent development, definition of scale-up criteria, and process design of a commercial size system. The APCI project is divided into eight separate tasks with an estimated duration of 16 months. This is the sixth monthly and second quarterly progress report.

Major emphasis this period has been in five areas:

1. Preparation of experimental sorbents
2. Dynamic tests of sorbents with different iron oxide sources
3. Derivation of differential equations to describe the dynamics of hydrogen sulfide sorption and sorbent regeneration
4. Solution of the differential equations which describe isothermal sorption
5. Comparison of the isothermal solution to the sorption dynamics equations with experimental data

II. EXPERIMENTAL WORK

A. Experimental Sorbents Prepared this Quarter

Table I lists the experimental sorbents prepared this quarter and enumerates their physical properties. A total of 13 experimental sorbents have been prepared. Seven were prepared with different iron oxide sources at the same 25% nominal iron oxide content and one-quarter inch pellet diameter.

TABLE I

PHYSICAL PROPERTIES OF IRON OXIDE/

FLY ASH SORBENTS PREPARED AS OF JANUARY 1976

FIXED PARAMETERS:

1. FORT MARTIN FLY ASH SUPPLIED BY ERDA-MERC
2. BENTONITE BINDER

VARIABLE PARAMETERS:

SORBENT CODE	Fe_2O_3 SOURCE	NOMINAL Fe_2O_3 ADDED	PELLET DIAMETER (INCHES)	CRUSHING STRENGTH (LB./MM.)	POROSITY (% H_2O ABSORPTION	BULK DENSITY (LG./L.)
705X8-5X1	FISCHER SCIENTIFIC	25	0.25	4.17	17.9	1.152
705X9-2X1	U.S. STEEL	25	0.25	5.43	16.1	1.184
705X10-1X1	J&L	25	0.25	3.72	20.4	1.031
705X11-1X5	ARMCO	25	0.25	6.46	17.4	1.115
705X12-1X3	U.S. STEEL	25	0.125	6.43	17.6	1.136
705X13-1X2	YOUNGSTOWN	25	0.25	3.6	18.8	1.113
705X14-1X2	REPUBLIC OPEN HEARTH	25	0.25	3.5	16.4	1.153
705X15-1X2	REPUBLIC BOF	25	0.25	4.4	19.8	1.067
800X1-1X2	U. S. STEEL	10	0.25	4.67	20.7	0.990
801X1-1X3	U. S. STEEL	15	0.25	4.58	19.7	1.012
801X2-1X2	U. S. STEEL	15	0.125	4.67	17.7	1.135
802X1-1X3	U. S. STEEL	20	0.25	7.47	18.0	1.079
803X1-1X2	U. S. STEEL	30	0.25	6.33	18.6	1.045

The other six sorbents were prepared with different nominal iron oxide contents and/or with one-eighth inch pellet diameter. Each of the 13 sorbents was heat treated differently to produce a pellet crushing strength greater than 3.5 pounds/mm. length and pellet porosity between 16 and 20%.

Table II lists this Laboratory's analysis of the seven iron oxide sources and the fly ash used to prepare the experimental sorbents in Table I. In some cases the analysis in Table I differs significantly from the suppliers typical analysis in Table IV, Quarterly Report No. 1. Major impurities in the iron oxide are ZnO in the Youngstown, J&L, and ARMCO sources and CaO in the Republic BOF source. The J&L Youngstown, and U.S. Steel sources contain more than 0.5 percent sulfur. All sources except Fischer Scientific contain significant levels of unknowns despite the fact that analysis was done for all impurities listed in the suppliers typical analysis.

The fly ash was found to consist mainly of SiO_2, Al_2O_3 and Fe_2O_3 as also reported in Bureau of Mines Report of Investigations 7947. The iron oxide in the fly ash could not be analyzed by X-ray fluorescence since it was bound in a matrix with SiO_2 and Al_2O_3. For this reason, fly ash iron oxide is assumed to contribute no sulfur sorption sites in the finished sorbent pellets.

The chemical analysis of the seven nominally 25 percent iron oxide experimental sorbents using different iron oxide sources is given in Table III. Each of these sorbents was prepared so that the added iron oxide calculated from the suppliers typical analyses was 25 percent. Added iron oxide as calculated from the analysis of Table II varies from 15 to 25 percent. Major impurities analyzed in the finished sorbents are the Al_2O_3 and SiO_2 contained in the fly ash. Amounts of ZnO and CaO impurities are consistent with the iron oxide source chemical analysis.

B. Dynamic Tests of Experimental Sorbents

1. Test Procedure

The unit used for dynamic testing of experimental sorbents was originally described in the Final Report for OCR Contract No. E(49-18)-1510, pages 5.1 to 5.15. The pertinent sections of that final report are included in Appendix B. This unit is herein referred to as the ERDA pressure unit.

A total of nineteen dynamic sorptions were conducted in the ERDA pressure unit this quarter. Each dynamic test was conducted by the following method:

TABLE II

CHEMICAL COMPOSITION OF IRON OXIDE SOURCES
AND FORT MARTIN FLY ASH

	← Iron Oxide Sources →							Fort Martin Fly Ash
	Fischer Sci	U.S. Steel	J&L	Armco	Youngstown	Republic OH	Republic BOF	
Composition								
Fe_2O_3	100.0	79.8	61.6	72.8	64.3	80.5	69.5	18.7
Sulphur		0.7	1.9	0.0	1.2	0.4	0.2	NA
Al_2O_3		0.7	0.6	0.6	0.8	0.5	0.7	24.4
ZnO		0.1	10.8	3.6	15.2	0.1	0.2	NA
CaO		0.4	0.6	0.2	1.0	0.9	11.1	NA
MgO		0.3	0.4	0.2	0.5	0.8	1.5	1.0
Na_2O		0.7	0.9	0.2	1.1	0.4	0.6	0.6
PbO		0.1	2.2	0.7	1.4	0.03	0.1	0.1
CuO		0.1	0.2	0.1	0.1	0.03	0.1	0.02
MnO		0.4	0.5	0.5	0.7	0.6	0.8	NA
Flourine		0.1	0.1	0.2	0.1	0.1	0.8	NA
TiO_2		NA	NA	NA	NA	NA	NA	0.4
K_2O		NA	NA	NA	NA	NA	NA	0.04
SiO_2 & Unknowns		16.4	20.4	20.9	15.6	14.3	14.3	54.7

NA = Not analyzed

All Analyses determined at Houdry Technical Center

TABLE III

CHEMICAL COMPOSITION OF SORBENT PELLETS

APCI Pellet Code No.	705x8-5x2	705x9-2x1	705x10-1x4	705x11-1x4	705x13-1x2	705x14-1x2	705x15-1x2
Iron Oxide Source	Fischer Scientific	U.S. Steel	J&L Steel	Armco	Youngstown	Republic Open Hearth	Republic BOF
Fly Ash Source	← Fort Martin Fly Ash Supplied by Bureau of Mines, Morgantown →						
Chemical Composition of Sorbent Pellets							
Added Fe_2O_3 (from iron oxide source)	25.0	20.0	15.5	20.9	16.0	20.9	18.9
Total Fe_2O_3	37.2	32.3	30.3	37.2	31.4	33.0	30.3
Sulfur	0.2	0.1	0.2	0.2	0.2	0.2	0.2
Al_2O_3	17.0	18.4	16.4	16.2	16.1	16.4	15.5
ZnO	0.02	0.1	2.6	1.1	4.3	0.1	0.1
CaO	0.2	0.1	0.2	0.2	0.2	0.2	1.1
MgO	0.9	0.9	0.9	0.8	0.9	1.0	1.2
Na_2O	0.6	0.7	0.7	0.6	0.8	0.6	0.7
PbO	0.0	0.02	0.6	0.2	0.4	0.0	0.04
CuO	0.01	0.04	0.1	0.04	0.1	0.02	0.04
MnO	0.04	0.1	0.1	0.2	0.2	0.2	0.2
Flourine	0.01	0.1	0.2	0.01	0.01	0.02	0.1
SiO & Unknowns	43.8	47.2	47.9	43.2	45.5	48.3	50.5

(1) Each test was a sorption of hydrogen sulfide on fresh experimental sorbent. Regenerations and sorptions on regenerated sorbents were not carried out.

(2) The tar and particulate free simulated low BTU producer gas feed to the ERDA pressure unit had the following nominal volumetric composition:

N_2	48.6%
CO	20.5%
H_2	14.9
CO_2	6.5%
CH_4	1.9%
H_2S	0.6%
H_2O	7.0%

(3) The hydrogen sulfide content of the offgas from the ERDA pressure unit was analyzed at 5 minute intervals by an automatic online GC unit. The test run was concluded after the concentration of the offgas equalled the feed gas hydrogen sulfide concentration for at least 2 hours.

(4) Sorbent capacities were determined by analysis of the spent experimental sorbents for total sulfur. An X-ray fluorescence technique was used for this analysis.

2. Initial Test Runs and Reproducibility

The first six dynamic test runs were conducted to achieve the following goals:

(1) Identify and correct operating problems with the ERDA pressure unit.

(2) To obtain the experimental reproducibility in measuring dynamic breakthrough curves.

Operating problems identified during these initial runs and corrective action taken are listed in Table IV.

TABLE IV

OPERATING PROBLEMS IDENTIFIED DURING
ERDA PRESSURE UNIT SHAKEDOWN RUNS

1. OPERATING PROBLEM

THE WATER FEED PUMP DID NOT MAINTAIN THE REQUIRED WATER FEED RATE OF 1 CUBIC CENTIMETER PER MINUTE WITHOUT CONSTANT OPERATOR ATTENTION.

CORRECTIVE ACTION

THE WATER FEED PUMP WAS REPLACED WITH A SMALLER CAPACITY MINIPUMP.

2. OPERATING PROBLEM

THE PROCESS FEED COIL IN THE RADIANT PREHEATER FAILED DUE TO HEAT STRESS AND/OR CORROSION.

CORRECTIVE ACTION

THE BREAK IN THE COIL WAS CLOSED WITH A WELD.

3. OPERATING PROBLEM

THE PROCESS GAS SAMPLE FLOW TO THE ONLINE G.C. WAS ERRATIC AND LOWER THAN THE FLOW SPECIFIED IN THE MANUFACTURERS OPERATING MANUAL.

CORRECTIVE ACTION

THE ERDA UNIT WAS OPERATED AT INCREASED PRESSURE (20 PSIG) TO INCREASE THE PROCESS GAS SAMPLE FLOW. A PROCESS GAS SAMPLE ROTAMETER WAS INSTALLED TO MONITOR FLOW RATES.

Figure 1 represents the results of three duplicate dynamic tests for sorbents prepared from the U.S. Steel iron oxide source. Nominal conditions of these runs are comparable to the conditions used for subsequent runs with different iron oxide sources. The ten percent breakthrough time for this series of dynamic tests is the onstream time for which the dimensionless hydrogen sulfide concentration of the sorbent bed offgas is 0.1; that is, the onstream time for desulfurization greater than 90%. From the dynamic tests of Figure 1, this time is observed to be 7.1 $\pm$ 0.8 hours. The uncertainty in measuring this breakthrough time is then indicated to be about 45 minutes. Other percent breakthrough times below 50% breakthrough have approximately the same or better experimental reproductibility.

3. Performance With Different Iron Oxide Sources

The goal of the remaining thirteen runs was to determine the effect of iron oxide source on sorbent performance. Breakthrough curves for four nominally 25% iron oxide sorbents with different iron oxide sources are shown in Figure 2. The nominal operating conditions for these runs and runs with other iron oxide sources are 1700 GHSV, 1200° temperature, 20 psig pressure, and 27 SCF/hr gas flowrate. These conditions were found to give differences in breakthrough between "good" and "poor" sorbents greater than the 45 minute experimental uncertainty described above. The dynamic tests shown in Figure 2 are typical in that most sorbents tested either performed well (ten percent breakthrough times between 6.0 and 7.5 hours) or poorly (breakthrough times less than 4 hours). Of the limited number of iron oxide sources investigated, U.S. Steel and Armco sources were found to be superior on the basis of this ten percent breakthrough time criteria. Since no dynamic tests on regenerated sorbents were conducted, all conclusions involving choice of iron oxide source apply to freshly prepared sorbents only.

Another criteria for judging dynamic sorbent performance will be demonstrated on page 28 of this report. This criteria makes use of the sorption dynamics model described in sections IIIB and IIIC to correct the experimental sorbents to 25 percent added iron oxide. The correction is needed since some of the sorbents containing nominally 25 percent added iron oxide have as little as 15 percent added iron oxide, see table III.

FIGURE 1

REPRODUCIBILITY OF SORPTION DYNAMICS

WITH SORBENT USING U.S. STEEL IRON OXIDE

NOMINAL CONDITIONS: 1800 GHSV, 20 PSIG,
1250°F, 0.7% H_2S FEED CONCENTRATION

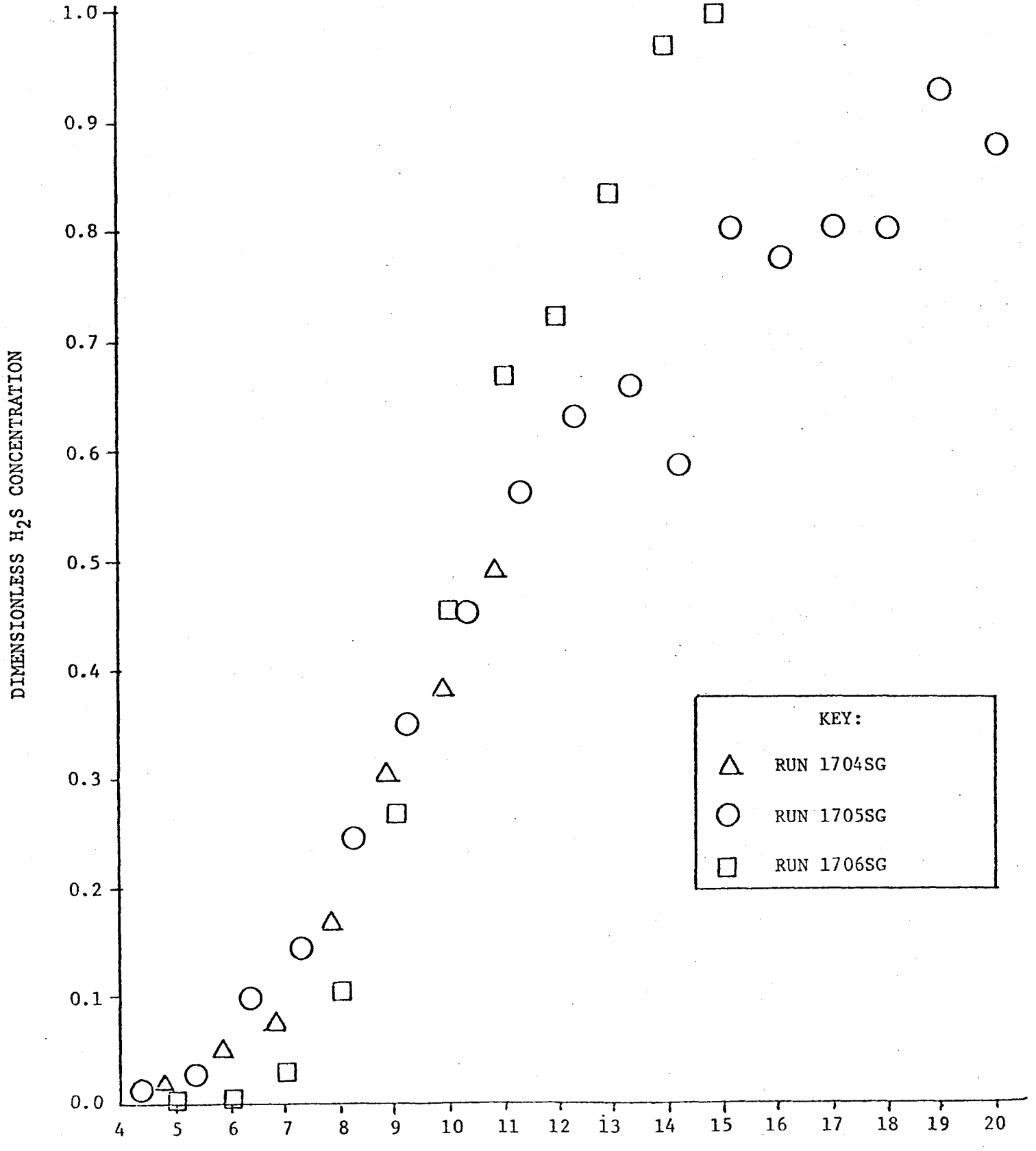

FIGURE 2

SORPTION DYNAMICS WITH DIFFERENT IRON OXIDE SOURCES

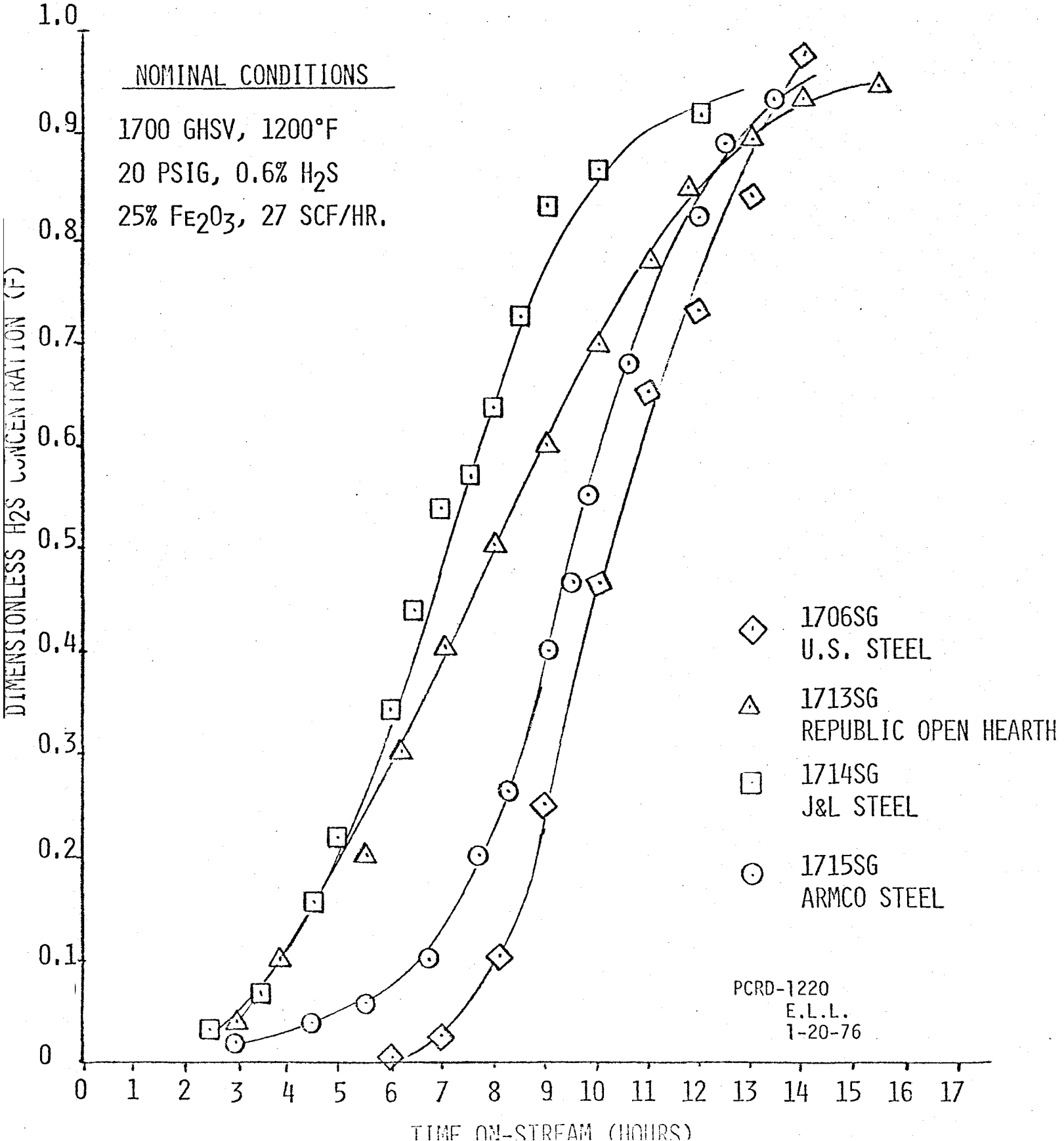

Finally, the amount of active iron oxide as determined by sulfur capacity per unit weight of source iron oxide is a criteria for iron oxide source selection. Table V illustrated the amount of active iron oxide in the sourcse tested. The required information on source iron oxide content and sorbent added iron oxide was presented in Table II and Table III of this report. Of the limited number of iron oxide sources investigated, U.S. Steel and Armco sources were found to have the largest sulfur capacities per weight of added source.

4. Preliminary Temperature Effect

Table VI illustrates two runs conducted to determine if temperature influenced sorbent performance. Both runs used the same sorbent, space velocity, and pressure. Run 1713SG was at 1200° F and run 1716SG at 1400° F. The higher temperature run indicated slightly increased sorbent sulfur capacity (4 relative percent) and significantly better dynamic performance (50% longer time to 10% breakthrough). These results need verification with additional dynamic tests.

III. SORPTION PROCESS MODEL

A. Objectives

The following objectives can be realized by a successful sorption process model:

1. Obtain a better understanding of the fundamentals of the process.

2. Consolidate all sorbent and process variables into a minimum number of pertinent dimensionless variables.

3. Obtain a reliable basis for scaling up experimental results.

4. Explore the effects of interactions of all variables.

TABLE V

CALCULATION OF SULFUR CAPACITY PER 100

GRAMS OF IRON OXIDE SOURCE

Iron Oxide Source	Grams Sulfur Sorbed Per 100 Grams of Spent Pellets	Added Grams Iron Oxide Per 100 Grams of Fresh Pellets	Weight Spent Pellets Per Weight Fresh Pellets	Grams Iron Oxide per 100 Grams of Source	Grams Sulfur Sorbed Per Gram of Added Iron Oxide	Grams Sulfur Sorbed Per 100 Grams of Source
U.S. Steel	10.5	20.0	1.062	79.8	0.558	44.5
J&L Steel	10.7	15.5	1.022	61.6	0.706	43.5
Armco Steel	13.2	20.9	1.017	72.8	0.642	46.7
Youngstown	9.5	16.0	1.033	64.3	0.613	39.4
Republic Open Hearth	10.1	20.9	1.026	80.5	0.496	39.9
Republic BOF	8.13	18.9	1.025	69.5	0.441	30.6

TABLE VI

TEMPERATURE EFFECTS ON SORPTION DYNAMICS

TEMPERATURE (°F)	1200	1400
SORBENT CODE	←——705X14-1X2——→	
SORBENT SOURCE	REPUBLIC OPEN HEARTH	
NOMINAL GHSV	←——1700——→	
NOMINAL VOLUME PERCENT H_2S	←——0.6——→	
NOMINAL SYSTEM PRESSURE, PSIG	←——20——→	
RUN NUMBER	1713SG	1716SG
BREAKTHROUGH TIMES (HOURS)		
10%	4.5	6.9
20%	5.5	7.8
SULFUR ANALYSIS OF SPENT SATURATED PELLETS (WEIGHT %)	9.7	10.1

B. Differential Equations for Sorption Dynamics

Four simultaneous partial differential equations are needed to describe the sorption of hydrogen sulfide on iron oxide/fly ash sorbents. These four equations are derived in the appendix and listed in Table VII. Nomenclature for Table VII is described in the appendix. The sorption dynamics equations may also be used to describe sorbent regeneration. This process is the sorption of oxygen on iron sulfide/fly ash particles.

The plan of attack for solving equations 1. through 4. of Table VII is summarized in Table VIII and explained below.

The mass balance equations 1. and 2 of Table VII are coupled to the energy balance equations (3. and 4.) through the dependence of physical properties (concentration, sorbent saturation level, and sorbate diffusivity) upon temperature. However, it is demonstrated in the appendix that if sorbent saturation level is not a function of temperature, then the mass balance equations listed above may be solved independently of the energy balance equations. The assumption of constant sorbent saturation level is reasonable if the method of H_2S sorption is an irreversible chemical reaction, such as:

$$\text{B1.}\quad Fe_2O_3 + 3\,H_2S \rightarrow 3\,H_2O + 2\,FeS_{1.5}$$

Since B1. is the assumed mechanism of sorption, the plan of attack for solving the system of partial differential involves solving the mass balance equations as a first step. This isothermal solution of the sorption dynamics equations will then be used to solve the energy balance equations.

The energy balance equations will be solved by obtaining simplified solutions through the use of restrictive assumptions and by then removing these assumptions one by one. The resulting procedure will provide information on a limiting case of the next computationally more difficult system of equations before that system has been solved. The most restrictive assumptions on the energy balance are that the temperature of a sorbent particle is uniform and equal to the temperature of the producer gas surrounding it. These assumptions reduce the energy balance to one equation with constant boundary conditions as indicated in the appendix. Solving the energy balance under these assumptions is thus the second step in the solution of the sorption dynamics equations. The solution of this step should be useful in predicting average bed temperature.

TABLE VII

SORPTION DYNAMICS EQUATIONS

1. ACCUMULATION OF HYDROGEN SULFIDE WITHIN SPHERICAL PARTICLE:

$$-N_{Ads}\frac{\partial \bar{z}}{\partial \tau} = \frac{F}{\bar{z}(1-\bar{z})}$$

2. DEPLETION OF HYDROGEN SULFIDE WITHIN PRODUCER GAS BETWEEN PARTICLES:

$$-N_{Ads}\frac{\partial F}{\partial X} = \frac{3F\bar{z}}{1-\bar{z}}$$

3. ACCUMULATION OF HEAT WITHIN SPHERICAL PARTICLE:

$$\frac{1}{R^2}\frac{\partial}{\partial R}\left(R^2\frac{\partial \theta}{\partial R}\right) = N_{P_E}\frac{\partial \theta_s}{\partial \tau}$$

4. ACCUMULATION OF HEAT WITHIN PRODUCER GAS:

$$\frac{\partial \theta_G}{\partial X} = -3N_{ST}\left[\theta_G - \theta_{S_{R=1}}\right]$$

TABLE VIII

PLAN OF ATTACK FOR SOLVING

THE SORPTION DYNAMICS EQUATIONS

I. SOLVE MASS BALANCE EQUATIONS FOR ISOTHERMAL BED.

II. USING THE SOLUTION TO THE MASS BALANCE EQUATIONS, SOLVE THE ENERGY BALANCE EQUATIONS FOR:

   A. UNIFORM PARTICLE TEMPERATURE EQUAL TO TEMPERATURE OF SURROUNDING PRODUCER GAS.

   B. UNIFORM PARTICLE TEMPERATURE UNEQUAL TO TEMPERATURE OF SURROUNDING PRODUCER GAS.

   C. NONUNIFORM PARTICLE TEMPERATURE UNEQUAL TO TEMPERATURE OF SURROUNDING PRODUCER GAS.

III. MODIFICATION OF RESULTING MODEL TO SOLVE DYNAMICS OF CYCLIC SORPTIONS AND REGENERATIONS.

The third step in the solution of these equations involves assuming that sorbent particle temperature is uniform but unequal to producer gas temperature. This assumption simplifies equation 4 of Table VII as indicated in the appendix. Finally, step four is to solve the full sorption dynamics equations for non-uniform sorbent particle temperature. Solution of these two steps is necessary to avoid regeneration conditions that could sinter the sorbent.

C. Isothermal Solution to the Sorption Dynamics Equations

For a nearly isothermal sorption the solution to the mass balance equations (1. and 2. of Table VII) should adequately describe the system sorption dynamics. Using the dimensionless variables described in the appendix, the isothermal solution leads to a breakthrough curve of normalized hydrogen sulfide concentration (F) vs. dimensionless time (τ) for each sorption number (N_{Ads}). Figure 3 is a computer generated solution of this type. The ordinant (F) is the hydrogen sulfide concentration of the producer gas leaving the bed divided by the inlet hydrogen sulfide concentration. This is the same as a normalized percent breakthrough. The abscissa (τ) is the real onstream time to a given breakthrough point divided by the stiochiometric time required for bed saturation if every sorbent particle were saturated before any hydrogen sulfide could exit the bed.

The time for complete bed saturation with zero breakthrough is referred to as the time for perfect sorption. It is the maximum onstream time prior to any breakthrough. A breakthrough curve for perfect sorption could be represented on Figure 3 by a vertical line at τ equals 1. The sorption number is a combination of pellet properties, linear velocity, and sorbent bed depth. Each sorption number characterizes a breakthrough curve such as Figure 3. Perfect sorption is characterized by a zero sorption number, a theoretical condition which can only be obtained with a sorbent bed of infinite length or a particle size of zero.

The concept of perfect sorption leads to another definition of τ; that of sorption efficiency. A sorbent has an efficiency of 1 if it can remove all sorbate from the feed gas until bed saturation. Since the situation described for an efficiency of 1 is perfect sorption, the efficiency of a sorption at a given breakthrough level is the ratio of breakthrough real time to perfect sorption time. This ratio is dimensionless time, τ.

The computer model developed to generate dimensionless breakthrough curves such as Figure 3 has been extensively tested for accuracy. This accuracy can be judged by the material balance closure: the amount of sorbate leaving in the effluent gas and the sorbate absorbed in the bed must

FIGURE 3

COMPUTER GENERATED SOLUTION TO SORPTION DYNAMICS

MASS BALANCE EQUATIONS FOR SORPTION NUMBER OF 5

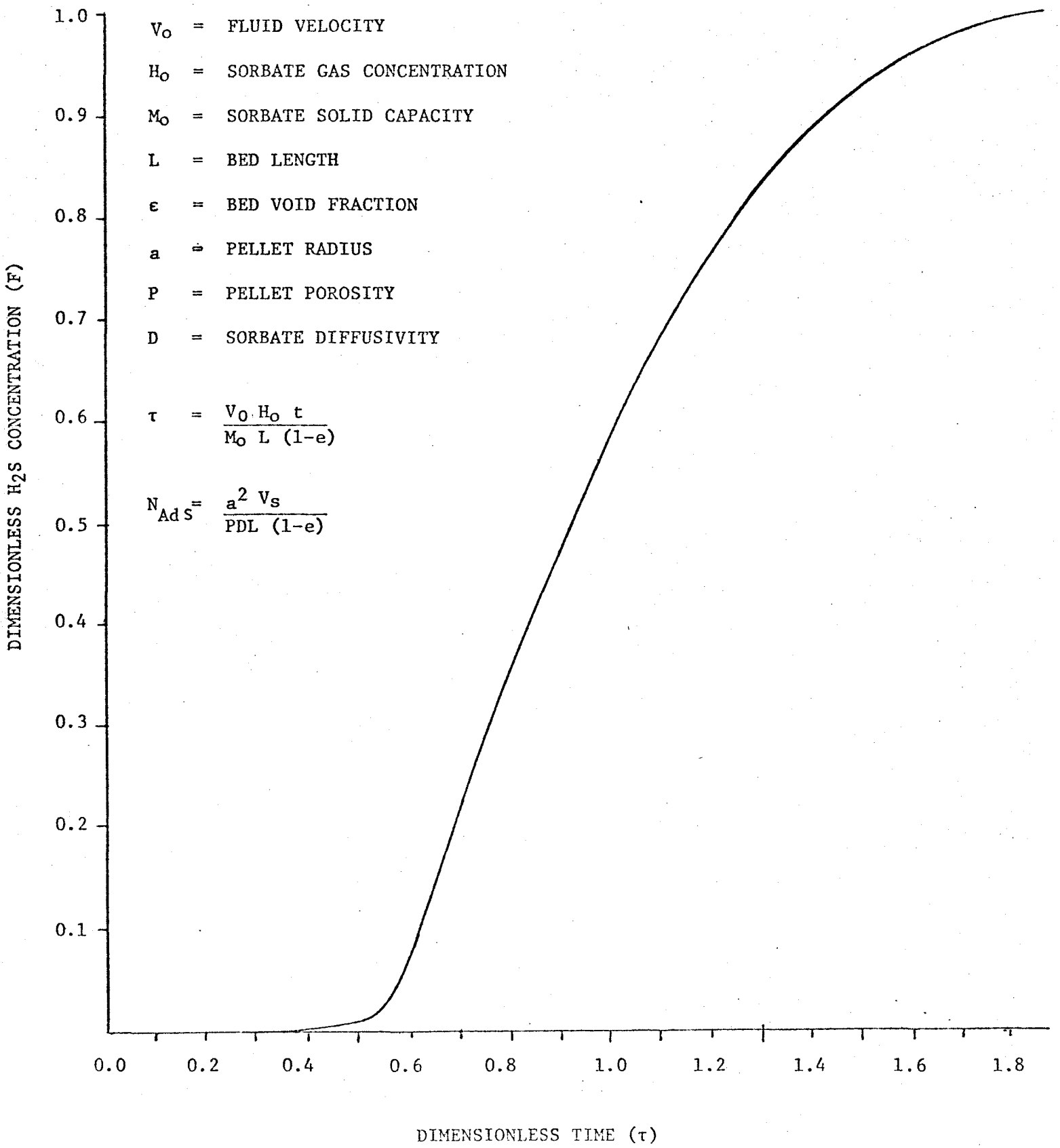

equal the sorbate fed to the system. Material balance closures were between 100 and 102% in all computer generated solutions.

The solution to the isothermal sorption dynamics equations can be fully illustrated in a chart such as Figure 4. This is a composite chart of the relationship among the three parameters used in the computer model. The ordinant is τ (sorption efficiency or dimensionless time), the abscisa is the sorption number, and percent breakthrough (F times 100%) is represented by contour lines.

D. Comparison of the Isothermal Solution to the Sorption Dynamics Equations with Experimental Data

The purpose of this section is to:

Show that the isothermal solution to the sorption dynamics equations fits the experimental breakthrough curves obtained from the ERDA pressure unit.

It has been demonstrated that the isothermal sorption solution predicts a breakthrough curve that is characterized by a single parameter, the sorption number. Figure 4, which represents this relationship, may be used to confirm that the sorption dynamics equations agree with experimental breakthrough data. The following procedure is used:

Step 1 - The time required for perfect sorption for the experimental run must be determined. This requires knowledge of the sorbent saturation level, the hydrogen sulfide concentration of the process gas, and the process gas flow rate. If this information is not available, Figure 4 indicates that for sorption numbers less than 10 the time for perfect sorption may be approximated by the 60 percent breakthrough time.

Step 2 - Dimensionless times for various breakthroughs are obtained by dividing the experimental time of breakthrough by the time for perfect sorption obtained in Step 1.

Step 3 - A plot of experimental percent breakthroughs versus experimental dimensionless times on Figure 4 should form a vertical line if the experimental sorption dynamics data agree with the computer generated solution to the sorption dynamics equation. This vertical line indicates that the experimental breakthrough curve is characterized by a single sorption number as predicted by the computer model.

Four experimental breakthrough curves were presented in Figure 2 representing four different absorbents. Percent breakthrough versus breakthrough time data from two of these curves is summarized in Table IX. In order to compare this experimental data with the solution to the isothermal sorption dynamics equations, breakthrough times must be converted to dimensionless times or chemical efficiencies. This is accomplished by dividing the real time by

FIGURE 4

COMPUTER GENERATED BREAKTHROUGH CURVES

FOR SORPTION NUMBERS BETWEEN ZERO TO THIRTEEN

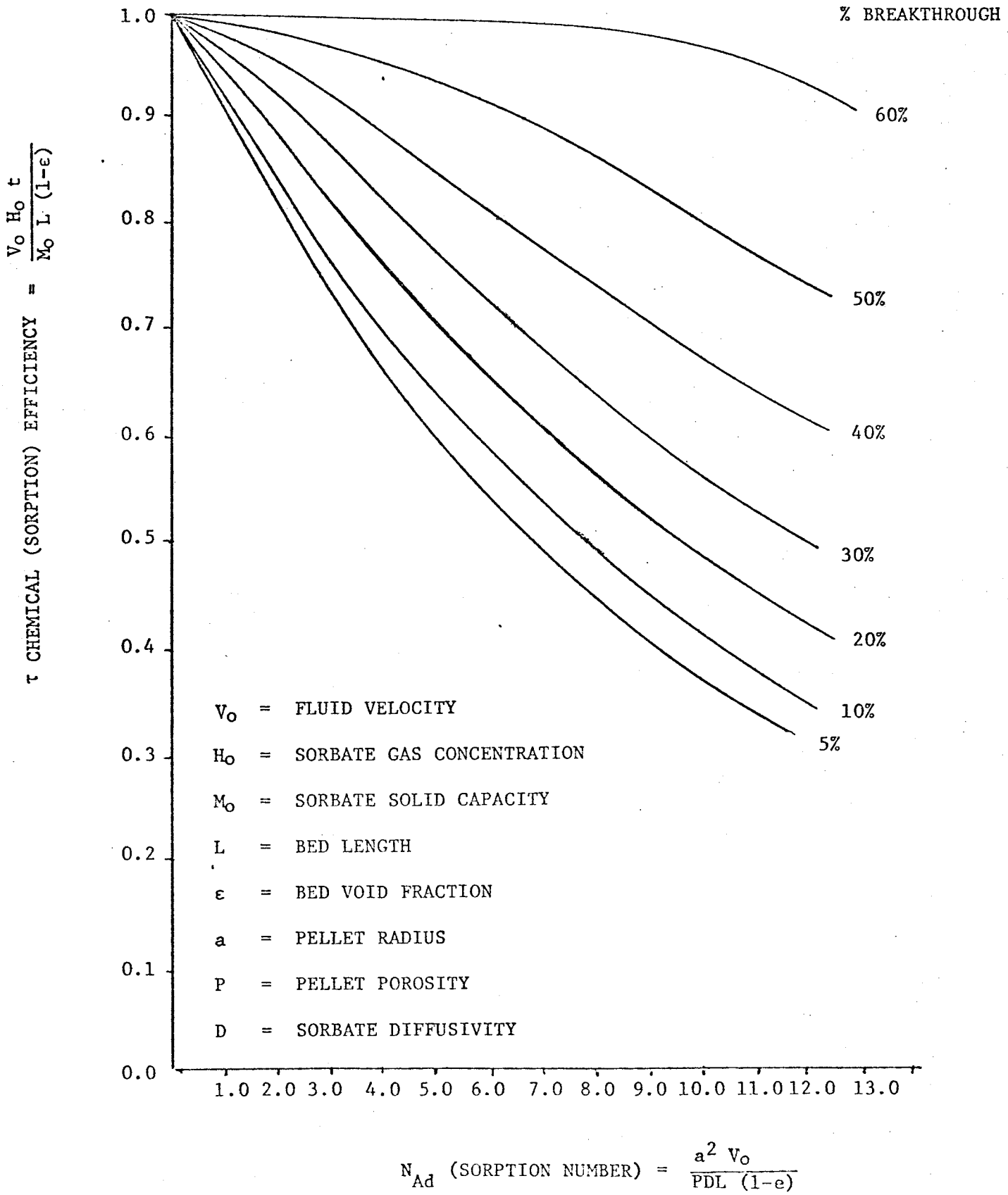

TABLE IX

DIMENSIONLESS SORPTION DYNAMICS DATA

FOR TWO DIFFERENT IRON OXIDE SOURCES

RUN NO.	1714SG		1715SG	
IRON OXIDE SOURCE	J&L STEEL		ARMCO STEEL	
NOMINAL CONDITIONS				
GHSV	1715		1745	
TEMPERATURE (°F)	← 1200 →			
H_2S VOLUME % OF FEED	← 0.59 →			
PRESSURE (PSIG)	← 21 →			
BREAKTHROUGH TIMES	HOURS	τ	HOURS	τ
10%	4.20	0.530	7.04	0.67
20%	5.00	0.632	7.88	0.76
30%	6.00	0.756	8.48	0.81
40%	6.50	0.821	9.21	0.88
50%	7.25	0.916	9.74	0.93
60%	8.08	1.020	10.37	0.99
SULFUR ON SPENT SATURATED SORBENT (WEIGHT PERCENT)	10.7		13.2	
TIME FOR PERFECT SORPTION (HOURS)	7.92		10.47	

the time for perfect sorption. Time for perfect sorption is calculated using the sulphur analysis of the spent saturated sorbent pellets and the feed rate of hydrogen sulfide to the sorbent bed. Resultant dimensionless time vs. percent breakthrough data is plotted on Figure 4.

Figure 5 is the result of this plot. The experimental breakthrough curves describe vertical lines on Figure 5. The dimensionless breakthrough curves for each dynamic test is therefore characterized by a single sorption number, confirming the validity of the isothermal sorption dynamics model.

E. Predicted Effects of GHSV and Pellet Properties

Figure 4 may also be used to determine the onstream time of a sorber. A sorber that must remove at least 90 percent of the hydrogen sulfide from a feed stream can only remain in service until its 10 percent breakthrough time. The 10% breakthrough curve of Figure 4 gives the relationship between the required dimensionless breakthrough time and sorption number. This relationship can be estimated from the equation:

$$E.1 \quad \tau_{10} = \exp\,(-0.09\ N_{Ads})$$

which is an empirical fit of the ten percent breakthrough curve. The definitions of dimensionless time and sorption number given in Table X can be substituted into equation E.1 to give a design equation for the sorber onstream time:

$$E.2 \quad t_{10} = \frac{Cap}{YH_2S.GHSV}\ EXP(-0.09N_{Pellet}.GHSV\ .CTP)$$

Nomenclature for equation D.2 is given in Table X. The design equation E.2 indicates that sorber onstream time is directly proportional to bed capacity and inversely proportional to the flow of hydrogen sulfide to the bed. The collection of sorbent properties in the pellet number reduce the onstream time exponentially, as does the gas hourly space velocity.

Figure 6 illustrates the effects of sorbent sulphur capacity and porosity diffusivity value on sorber onstream time for 10% breakthrough at constant GHSV. The constant parameters for Figure 6 are those of the dynamic test runs for experimental sorbents with different iron oxide sources:

GHSV = 1700 hr^{-1}
Feed Gas H_2S volume percent = 0.6%
Sorbent bulk density = 1.1 kg/l
Bed void fraction = 0.4
Pellet diameter = 0.25 inches

The remaining variable parameter for Figure 6 is the product of pellet porosity and pore diffusivity. Figure 6 demonstrates that for constant pellet properties, the sorption dynamics model predicts that the time to

FIGURE 5

COMPARISON OF MODEL AND EXPERIMENTAL

BREAKTHROUGH CURVES FOR J&L AND ARMCO IRON OXIDE SOURCES

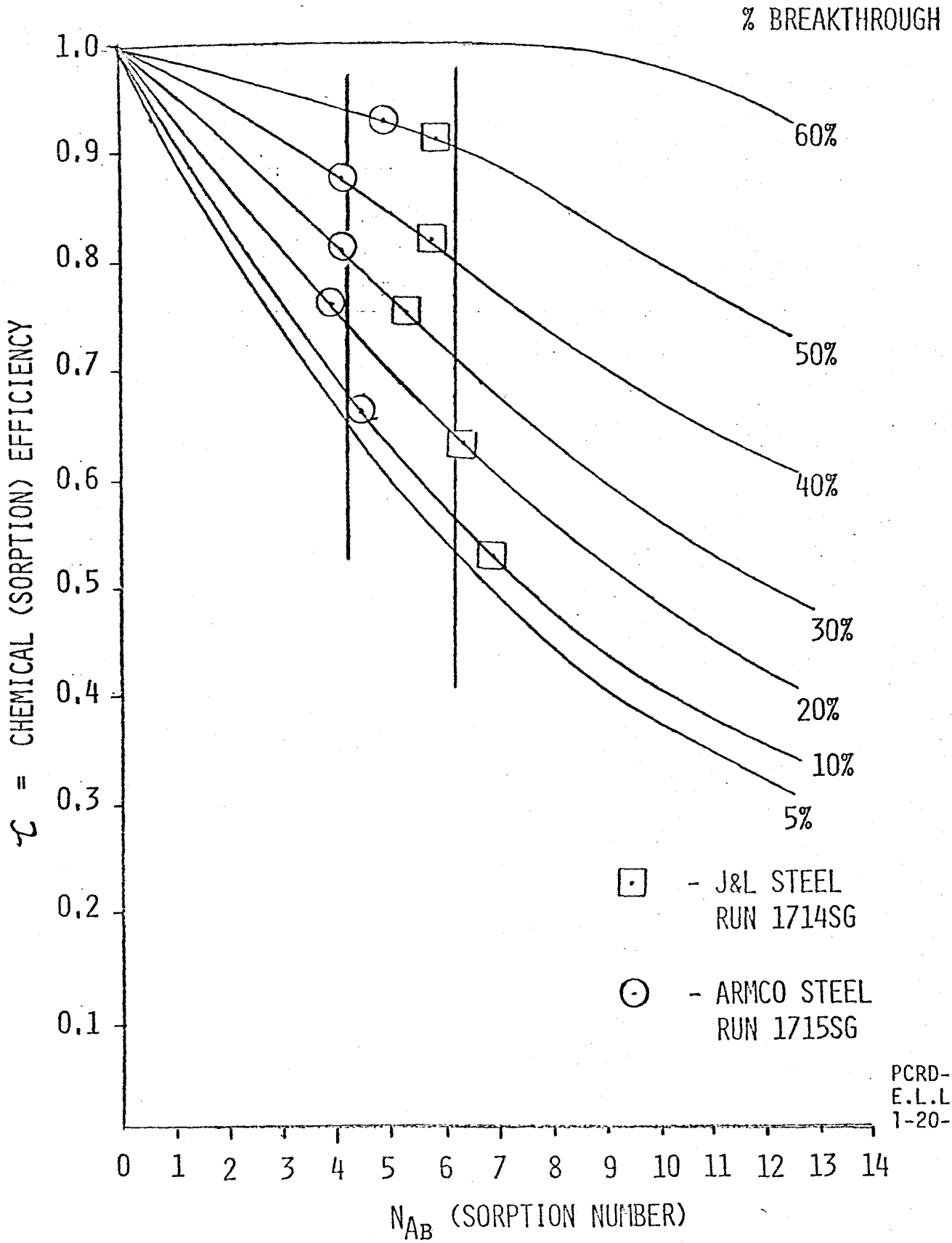

TABLE X

SORPTION EFFICIENCY AND SORPTION NUMBER

EXPRESSED IN TERMS OF DESIGN VARIABLES

$$\tau_{10} = \frac{t_{10} \cdot Y_{H_2S} \cdot GHSV}{Cap}$$

$$N_{Ads} = \frac{a^2 V_o}{PD(1-E)L} = N_{Pellet} \cdot GHSV \cdot CTP$$

Nomenclature:

a	Sorbent pellet radius (ft.)
Cap	Sorbent H_2S capacity (SCF H_2S/CF bed)
C_{TP}	Temperature and pressure correction for converting gas volume at STP to process conditions.
D	Sorbent diffusivity (ft^2/hr, must be determined experimentally)
E	Sorbent bed void fraction (vol/Vol)
GHSV	Gas hourly space velocity at STP
L	Bed depth (ft.)
N_{Ads}	Sorption Number (dimensionless)
N_{Pellet}	Pellet Number based on pellet properties $a^2/PD(1-E)$ (hr.)
P	Pellet volumetric porosity (dimensionless)
t_{10}	Ten percent breakthrough time (hrs.)
τ_{10}	Ten percent sorption efficiency
Vo	Superficial velocity at process conditions (ft/hr)
Y_{H_2S}	Volume fraction H_2S in feed gas.

FIGURE 6

EFFECT OF SORBENT SULFUR CAPACITY ON 10% BREAKTHROUGH TIME AT CONSTANT GHSV

Constant Parameters: 1700 GHSV, 0.6% H_2S in feed, 0.25 inch pellet diameter
Bed Density = 1.1 kg/l, E=0.4, Pressure = 20 psig, Temperature = 1200°F
Weight % Sulfur in spent saturated sorbent Ctp = 1.43

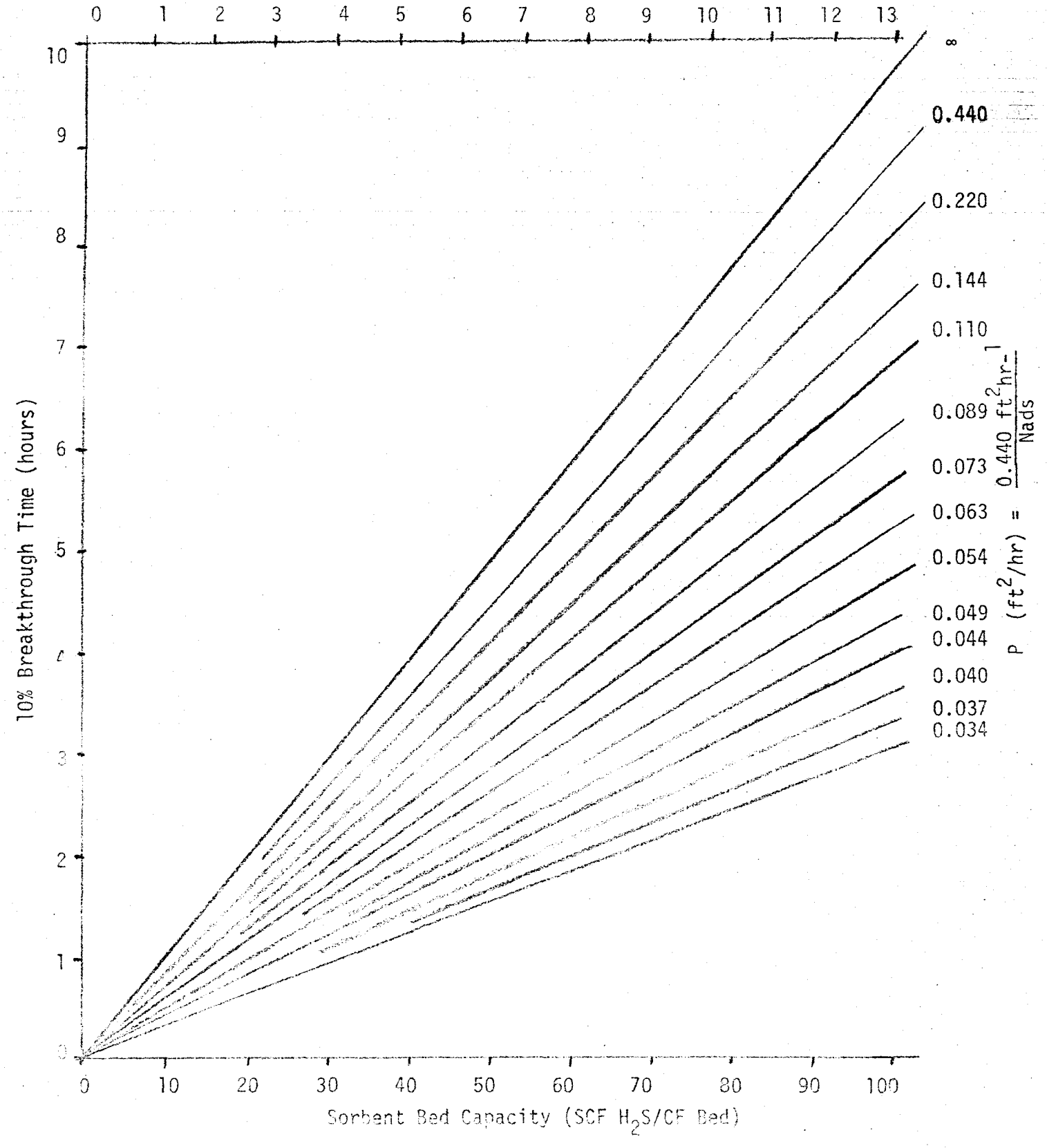

ten percent breakthrough is directly proportional to sorbent capacity. If sorbent capacity for sulphur is proportional to the added iron oxide content of the sorbent then Figure 6 also illustrates the effects of added iron oxide on 10 percent breakthrough time for constant pellet properties. Finally, Figure 6 shows that higher pore diffusivities favor better sorbent performance. The effect of increased porosity diffusivity value is large at low levels of porosity diffusivity and minor at high levels. An infinite porosity diffusivity value approaches perfect sorption operation.

Figure 7 shows the effects of GHSV and pellet number on the 10% breakthrough time predicted by the sorption dynamics model. It is obvious that high GHSV leads to very poor sorbent performances due to the increased flow of sorbate through the system (since the percentage of H_2S in the feed is held constant) and due to an adverse effect on sorption efficiency. In other words, increasing the GHSV both decreases the time for perfect sorption and decreases the sorption efficiency. For low GHSV (less than 1500 on Figure 7), the reduction of perfect sorption time is the most significant effect of increasing GHSV. In this region sorbents with high pellet numbers have nearly as lengthy onstream times to 10% breakthrough as those with low pellet numbers. For example, at 1000 GHSV Figure 7 indicates an 8 fold decrease in pellet number will increase the 10% breakthrough time from 13 to 20 hours, a small change relative to the change in the pellet number. At high GHSV (above 1500 on Figure 7), a small pellet number is essential for reasonable lengthy onstream times. In this region the effect of GHSV on perfect sorption time has already substantially reduced the maximum sorption time to 10% breakthrough. The GHSV effect on sorption efficiency at these high GHSV's coupled with a high pellet number can lead to very short breakthrough times. For example, at 4000 GHSV Figure 7 indicates that an 8 fold decrease in the pellet number can reduce the ten percent breakthrough time from 4 hours to one hour.

Figure 8 illustrates the effects of GHSV and pellet number on sorption efficiency. As mentioned in the preceding discussion, very low sorption efficiencies are predicted at high GHSV and high pellet numbers.

F. Pellet Diffusivity From Dynamics Test

The isothermal sorption dynamics model may now be used to determine which iron oxide source demonstrates the best dynamic performance. It is assumed that the pore diffusivity of an experimental sorbent is dependent principally on the iron oxide source. Pore diffusivity must then be a major criteria for selecting the best iron oxide source.

Figure 9 is a plot of 10% breakthrough time vs. sorbent capacity for several pore diffusivities. This graph was developed as Figure 6 in Section III E pg.27. The circles on Figure 9 represent dynamic data from test runs using sorbents with diffent iron oxide sources. Figure 9 shows that sorbent performance increases with pore diffusivity. The experimental points on Figure 9 indicate that the following iron oxide sources have high diffusivities:

(1) U.S. Steel

FIGURE 7

ESTIMATED 10% BREAKTHROUGH TIMES VERSUS GHSV FOR SEVERAL PELLET NUMBERS AT CONSTANT CAPACITY NUMBER

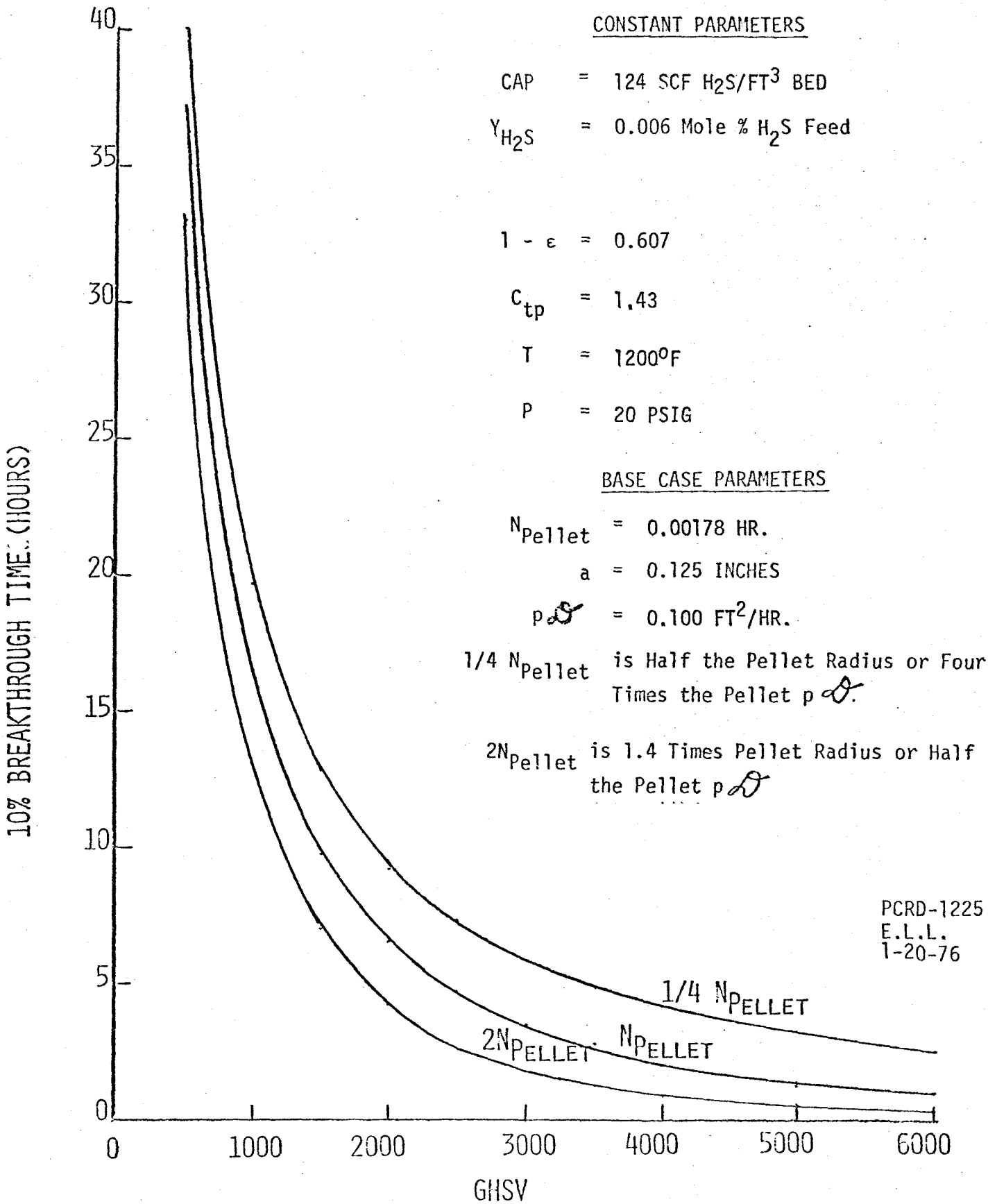

CONSTANT PARAMETERS

CAP = 124 SCF H_2S/FT^3 BED

Y_{H_2S} = 0.006 Mole % H_2S Feed

$1 - \varepsilon$ = 0.607

C_{tp} = 1.43

T = 1200°F

P = 20 PSIG

BASE CASE PARAMETERS

N_{Pellet} = 0.00178 HR.

a = 0.125 INCHES

$p\mathcal{D}$ = 0.100 $FT^2/HR.$

$1/4\ N_{Pellet}$ is Half the Pellet Radius or Four Times the Pellet $p\mathcal{D}$.

$2N_{Pellet}$ is 1.4 Times Pellet Radius or Half the Pellet $p\mathcal{D}$

PCRD-1225
E.L.L.
1-20-76

FIGURE 8

ESTIMATED SORPTION EFFICIENCY AT 10% BREAKTHROUGH VS. GHSV
FOR SEVERAL PELLET NUMBERS AT CONSTANT CAPACITY

CONSTANT PARAMETERS

Cap = 124 SCF H_2S/FT^3 BED
Yo = 0.006 MOLE % H_2S FEED
$1-\varepsilon$ = 0.607

CTp = 1.43
T = 1200°F
P = 20 PSIG

BASE CASE PARAMETERS

N_{pellet} = 0.00178 HRS.
R = 0.125 INCHES
$p\mathscr{D}$ = 0.100 FT^2/HR.

¼ N_{pellet} IS HALF THE PELLET RADIUS OR FOUR TIMES THE PELLET $p\mathscr{D}$

2 N_{pellet} IS 1.4 TIMES THE PELLET RADIUS OR HALF THE PELLET $p\mathscr{D}$

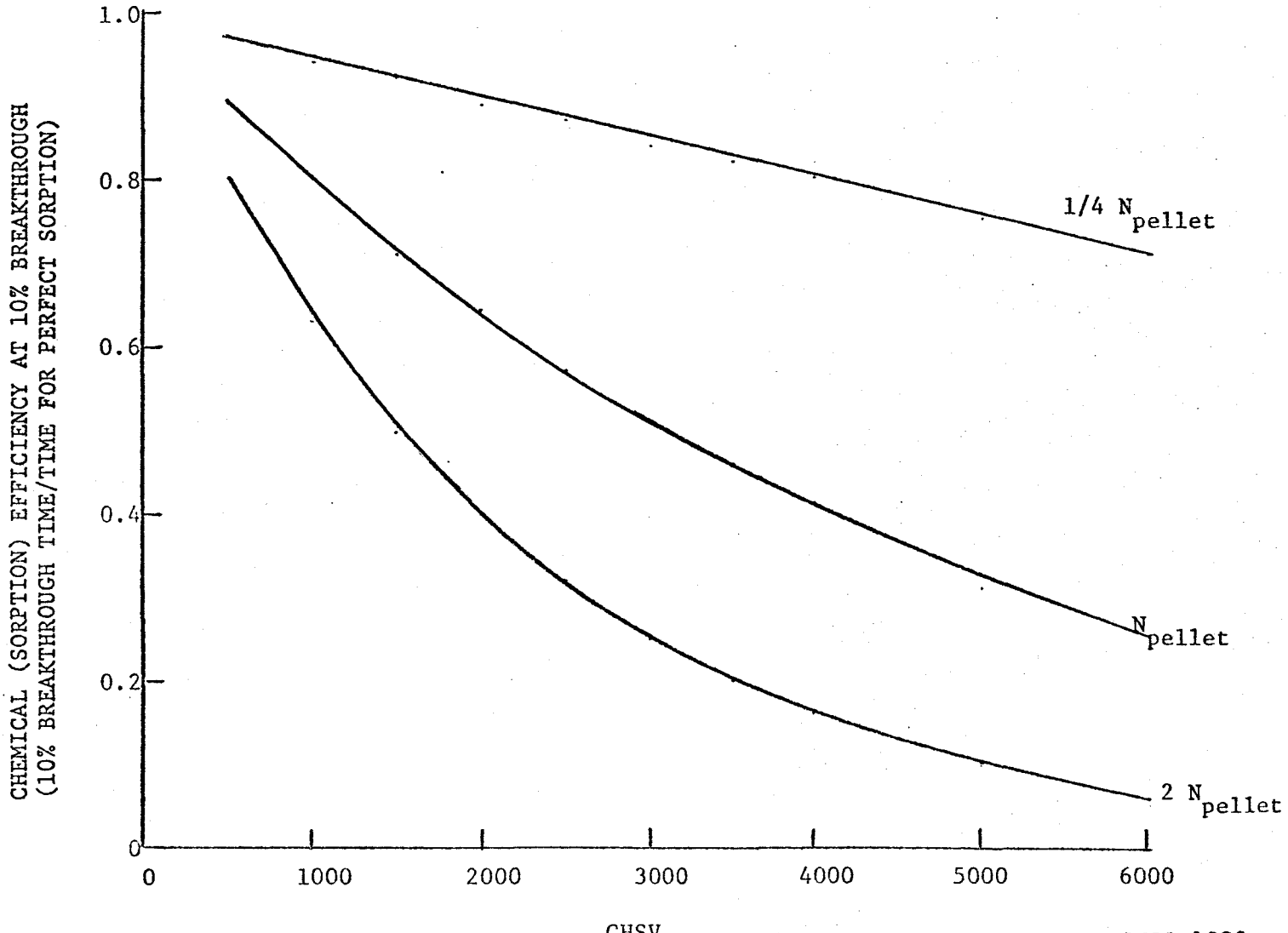

PCRD-1226
E.L.L.
1-20-76

FIGURE 9

PORE DIFFUSIVITIES OF SORBENTS USING DIFFERENT IRON OXIDE SOURCES AS DETERMINED BY 10% BREAKTHROUGH TIME AND SULFUR CAPACITY

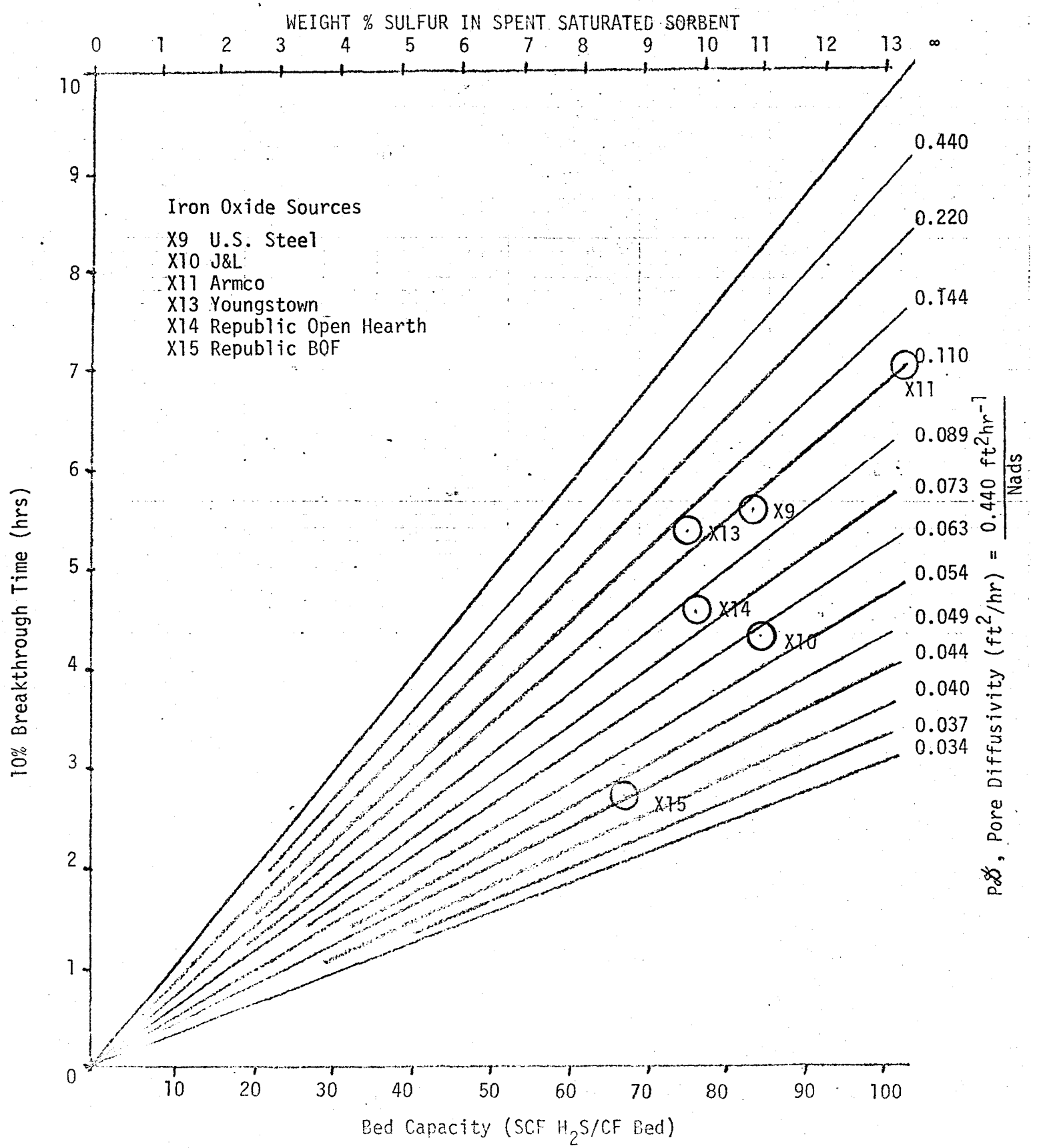

(2) Armco Steel

(3) Youngstown Steel

Thus, from the standpoint of pore diffusivity, three of the limited number of iron oxide sources investigated are superior.

In choosing an iron oxide source for sorbent manufacture, the sulphur capacity per unit weight of added iron oxide should also be considered. This information is presented in Section II B.3, Table V. U.S. Steel and Armco Steel sources have the highest capacities (45 grams sulphur per 100 grams source). Thus, of the limited number of iron oxide sources investigated, U.S. Steel and Armco Steel sources are superior according to the sulfur capacity criteria and the pore siffusivity criteria. These criteria have been investigated for sorption on freshly prepared sorbents only and need further evaluation by life study testing.

IV. PRELIMINARY DESIGN OF A SORBER USING ISOTHERMAL SORPTION MODEL

This section demonstrates the applicability of the results obtained this quarter to commercial sorber design. Suppose the following criteria are desired for a commercial sorber design to process low BTU producer gas:

(1) Sorber Capacity: 120 MSCFH Producer Gas

(2) Minimum Onstream Time: 10 hours to 10% breakthrough

(3) Maximum Allowable Sorber Pressure Drop: 8 psi

(4) Bed Inlet Pressure: 150 psig

(5) Bed Temperature: 1200°F

It was determined in Section III F that suitable sorbents have a porosity times diffusivity of 0.110 ft^2/hr and a capacity of 80 SCF H_2S per CF of bed at the 20% added iron oxide level. Suppose the further work indicates that at the 30% added iron oxide level this sorbent has a $p\mathcal{D}$ of 0.100 ft^2/hr and a capacity of 120 SCF H_2S/CF of bed. Finally, assume that the 30% level of added iron oxide is the highest possible level on the basis of acceptable sorbent hardness. Table XI is a listing of sorber onstream time as a function of space velocity for the assumed sorbent properties at the 30% added iron oxide level. This table was developed using design equation E.2.

$$E.2\quad \tau_{10} = \frac{CAP}{YH_S.GHSV}\ EXP\ (-0.09\ N_{Pellet}.GHSV.C_{TP})$$

TABLE XI

ESTIMATE OF 10% BREAKTHROUGH TIMES FOR

SORBENT WITH 30% ADDED U.S. STEEL IRON OXIDE

BED CAPACITY (SCF H_2S/CF BED)	120.
H_2S VOLUME % IN FEED	0.6
BED VOID FRACTION	0.4
$\frac{CTP}{\rho\sigma}$ (Determined at 1200°F, 20 psig, and assumed pressure independent for this example, units: ft^2 hr)	14.3

PELLET DIAMETER, INCHES	0.25	0.125
GHSV	t_{10} (hours)	
500	37.0	40.3
1000	16.5	19.6
1500	9.8	12.7
2000	6.6	9.2
2500	4.7	7.2
3000	3.5	5.8
3500	2.7	4.8
4000	2.1	4.1
5000	1.3	3.1
6000	0.9	2.5

The onstream times in Table XI are strictly applicable only at 1200°F and 20 psig pressure. For the purpose of this example, it is assumed that the CTP to pore diffusivity ratio is not a function of pressure. This is a valid assumption if the diffusional process is molecular diffusion limited. Table XI is then appropriate to determine the sorber onstream time for the commercial design criteria. The GHSV vs. 10% breakthrough time information indicates a GHSV of 1500 or less is needed for onstream time to be ten hours or more for both particle sizes. Note that if the minimum onstream time was 4.7 hours, the space velocity would be 2500 for one-quarter inch pellets and 3500 for one-eighth inch pellets. This further demonstrates the critical effect of pellet number on sorption efficiency at high GHSV discussed in Section III E, page 28 .

Since the required GHSV for the sorber is 1500 and the sorber capacity is 120,000 SCF/hr, the sorber bed volume required is 80 cubic feet. The allowable pressure drop of 8 psi is now used to determine sorber dimensions. Figure 10 shows the results of pressure drop calculations for several GHSV and several diameters at constant sorber capacity using the Ergun equation. Pressure drop calculations indicate that the sorber should be approximately 3 feet in diameter and 11 feet high for a one-eighth inch pellet diameter. The same size sorber would have less than 4 psi pressure drop for quarter inch pellets.

The pilot plant sorber located at the Morgantown Energy Research Center was designed to operate according to the criteria used in this section. It is 3 feet in diameter and can accommodate up to 17 feet of sorbent bed. The onstream times and pressure drops estimated above may be considered estimates of the MERC pilot sorber performance. Table XII summarizes the sorber design information calculated in this section.

V. PLANS FOR NEXT QUARTER

Emphasis during next quarter will be placed in the following areas;

1. Preparation of experimental sorbents

   Remaining Task I and II sorbents will be prepared.

2. Dynamic tests of experimental sorbents

   All Task I and II dynamic tests will be concluded.

3. Confirmation of isothermal sorption model

   The isothermal model will be used to predict the results of Task II dynamic tests. Predicted and experimental results will be compared.

FIGURE 10

ESTIMATED EFFECTS OF MAXIMUM PRESSURE DROP
AND PARTICLE SIZE ON SORPTION VESSEL DESIGN

NOMINAL VESSEL PRESSURE	150 PSIG
POWER PLANT CAPACITY	2.1 MW
GAS RATE	120 M SCFH
PRESSURE DROP CALCULATIONS	ERGUN EQUATION

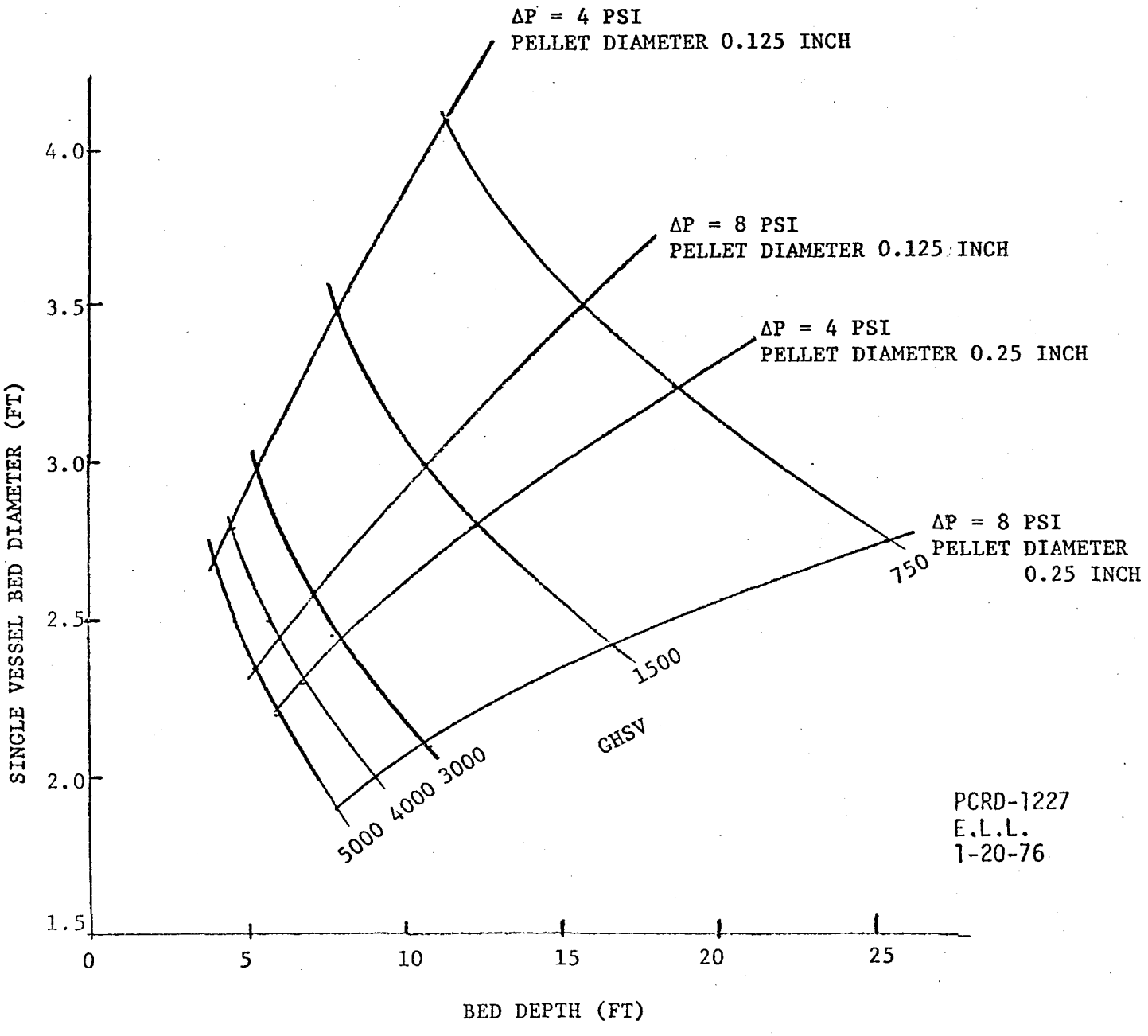

TABLE XII

ESTIMATED EFFECTS OF SORBENT PELLET SIZE AND

MAXIMUM BED PRESSURE DROP ON HIGH PRESSURE SORBER DESIGN

CAPACITY, MW	← 2.1 →			
GAS RATE, M SCFH	← 120 →			
NOMINAL PRESSURE, PSIG	← 150 →			
GHSV (STP)	← 1500 →			
PELLET DIAMETER (INCHES)	← 0.125 →		← 0.25 →	
TIME TO 10% BREAKTHROUGH, HOURS (Ignoring effects of pressure)	← 13.0 →		← 10.0 →	
MAXIMUM BED ΔP, PSI	4	8	4	8
BED DEPTH, FEET	7.8	10.5	12.1	16.7
BED DIAMETER, FEET	3.6	3.1	2.8	2.5

4. Programming of non-isothermal sorption model for Task III

Heat balance will be added to the isothermal model to predict sorbent regeneration heat effects.

5. Confirmation of non-isothermal model

The Task III non-isothermal model will be compared with ERDA-MERC sorbent regeneration tests.

6. Dynamic Coking Tests

Experimental work for task VI will be begun.

APPENDIX A

DERIVATION OF DIFFERENTIAL EQUATIONS TO DESCRIBE THE DYNAMICS OF HYDROGEN SULFIDE SORPTION ON IRON OXIDE/FLY ASH SORBENTS

APPENDIX A

DERIVATION OF DIFFERENTIAL EQUATIONS TO DESCRIBE THE DYNAMICS OF HYDROGEN SULFIDE SORPTION ON IRON OXIDE/FLY ASH SORBENTS

I. OBJECTIVES

The differential equations developed are appropriate for hydrogen sulfide sorption and regeneration. The objectives of this effort are as follows:

1. Obtain a better understanding of the fundamentals of the process.
2. Consolidate all sorbent and process variables into a minimum number of pertinent dimensionless variables.
3. Obtain a reliable basis for scaling up experimental results.
4. Explore the effects of interactions of all variables.

II. THE SHRINKING CORE MODEL

The model developed to describe the behavior of a single spherical sorbent particle is based on the shrinking core or shell type mechanism. The particle consists of two distinct solid phases with this mechanism: an outer shell phase that is 100% reacted, and an inner core that is 100% unreacted. Reaction of sorbent with sorbate hydrogen sulfide occurs solely at the interface between the outer shell and the inner core. As the reaction proceeds, the inner core shrinks; thus the sorbtion model is called a shrinking core model. Figure 1 illustrates the shrinking core model for sorption in a spherical particle of radius a and radial interface z. For sorption the outer shell represents $FeS_{1.5}$/fly ash and the inner core iron oxide/fly ash. For regeneration, the outer shell represents iron oxide/fly ash and the inner core $FeS_{1.5}$/fly ash.

III. ASSUMPTIONS

1. The gas-solid reaction rate is infinitely fast.
2. The concentration of H_2S at the interface shown in Figure 1 is zero due to the fast reaction assumed.

FIGURE 1

SHELL ABSORPTION MODEL

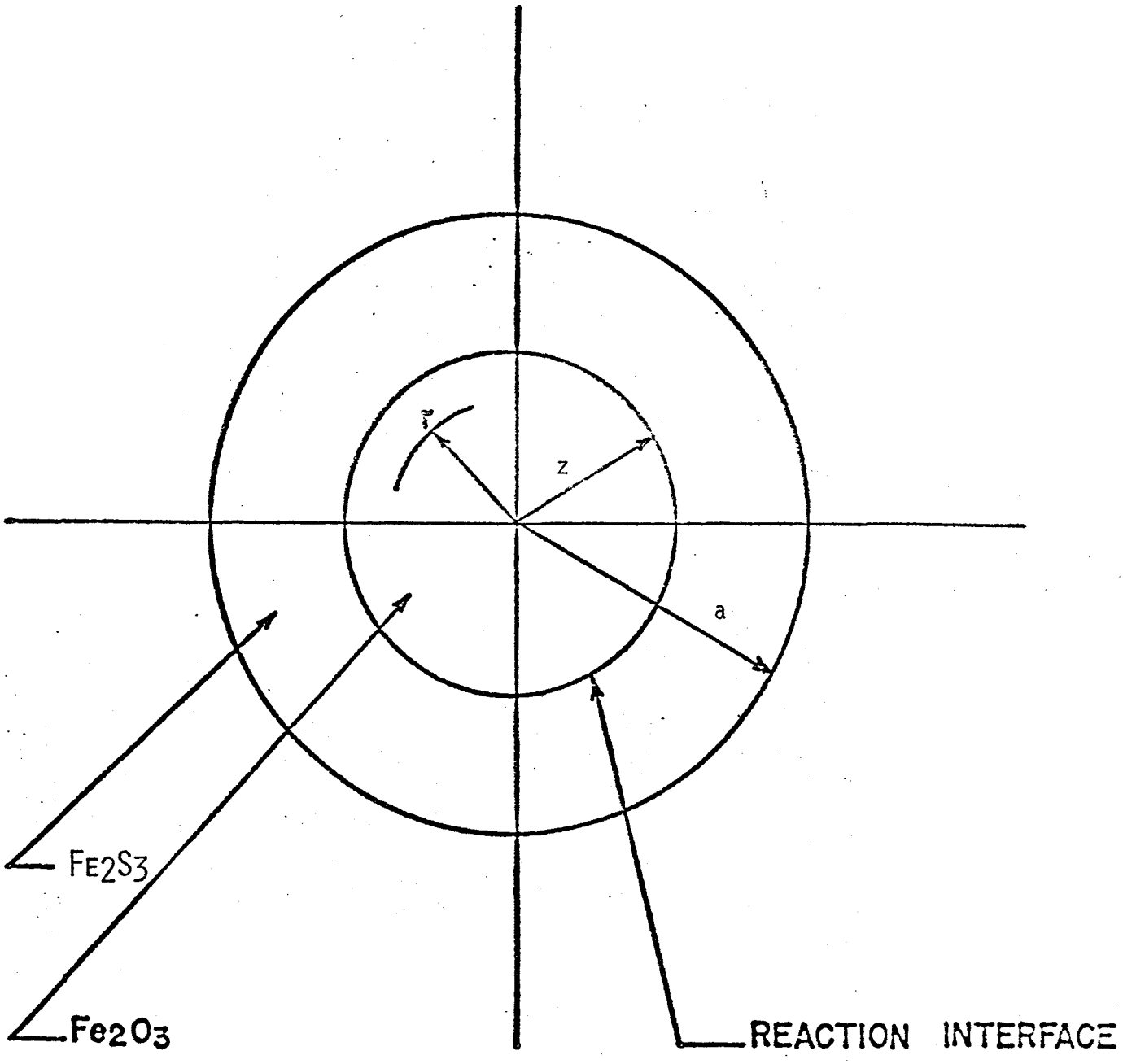

APPENDIX A

3. The reaction is not equilibrium limited. (Sorbent saturation level is not affected by temperature changes or concentration changes.)

4. Mass transfer resistance in the bulk phase exterior to the particle is negligible.

5. Gas flow through the sorbent bed is plug flow.

6. The product of pore diffusivity and gas concentration ($\mathscr{D}f$) is a constant. Since concentration is inversely proportional to temperature, this assumption is equivalent to assuming pore diffusivity proportional to temperature.

IV. NOMENCLATURE

Table A1 lists the nomenclature used in the following sections of this development.

V. PARTICLE MASS BALANCE EQUATION

Referring to Figure 1; the mass balance for the sorbate H_2S concentration in the outer unreacted shell is constructed as follows:

$$\text{Input} = \text{Output} + \text{Reacted} + \text{Accumulated} \tag{1}$$

The rate at which sorbate travels into a porous differential element of outer shell is:

$$\text{Input} = -4\pi r^2 \, p \mathscr{D}f \, \frac{\partial x}{\partial r} \tag{2}$$

The rate at which sorbate leaves the differential element is:

$$\text{Output} = -4\pi r^2 \, p\mathscr{D}f \, \frac{\partial x}{\partial r} + \frac{\partial}{\partial r}\left(-4\pi r^2 \, p\mathscr{D}f \, \frac{\partial x}{\partial r}\right) \partial r \tag{3}$$

Since the shrinking core model assumes the outer shell is 100% reacted, no reaction can occur in the differential element

$$\text{Reacted} = \text{Zero} \tag{4}$$

TABLE A1

NOMENCLATURE

DIMENSIONLESS GROUPINGS

1. $N_{Ad} = \frac{a^2 V_o}{(1 - E) \mathscr{D}_{oL} p}$ — Adsorption Number

2. $N_{H_R} = \frac{\Delta H_r p \mathscr{D}_o f_o X_{Go}}{T_o k_s}$ — Dimensionless Heat of Reaction

3. $N_{Nu} = \frac{h a}{k_s}$ — Nusselt Number for Particle

4. $N_{Pe} = \frac{a^2 \rho_s C_{Ps} V_o}{L k_s} \frac{f_o X_{Go}}{M_o (1 - E)}$ — Peclet Number Divided by Dimensionless Saturation Level of Sorbent

5. $N_{st} = \frac{(1 - E) L}{a} \frac{h}{\rho_{Go} C_{P_G} V_o}$ — Stanton Number

6. $\tau = \frac{V_o f_o X_{Go} t}{L (1 - E) M_o}$ — Chemical Efficiency

SYSTEM VARIABLES AND PROPERTIES

a	Adsorbent pellet radius (ft)
Cp	Heat capacity (Btu/lb ^oF)
$\mathscr{D}$	Pore diffusivity (ft^2/hr)

TABLE A1

NOMENCLATURE

(Continued)

E	Bed void fraction (ft^3/ft^3)
F	Dimensionless adsorbate concentration (X_G/X_G^o)
f	Gas density (lb moles/ft^3)
g	Number of spherical particles per ft of bed (ft^{-1})
h	Film convective heat transfer coefficient (Btu/ft^2 hr ^oF)
ΔH_r	Heat of adsorption (negative for exothermic adsorption) (Btu/lb mole)
k	Thermal conductivity of adsorbent (Btu/ft hr ^oF)
L	Total bed length (ft)
ℓ	Distance in bed from inlet (ft)
M^o	Equilibrium adsorbate capacity of adsorbent (lb moles) adsorbate/ft^3 adsorbent)
N	Reaction rate per sorbent particle (lb moles/hr)
p	Adsorbent porosity (in^3/in^3)
r	Distance from adsorbent pellet center (ft)
ρ	Density (lb/ft^3)
T	Temperature (^oF)
Θ	Dimensionless temperature (T/T^o)
t	Time (hr)
V	Superficial velocity (ft/hr)
R	Dimensionless distance from pellet center (r/a)
Z	Dimensionless distance of reaction zone from pellet center $\left(\frac{z}{a}\right)$
z	Distance of reaction zone from pellet center (ft)

TABLE A1

NOMENCLATURE

(Continued)

X	Dimensionless bed length $\left(\frac{\ell}{L}\right)$
x	Sorbate mole fraction within particle (dimensionless)

SUBSCRIPTS

G	Gas phase
O	Initial conditions
S	Solid adsorbent phase

APPENDIX A

Since the change of inventory of the sorbate in the porous space is usually very small compared to the difference in diffusive flow into and out of the differential element, the accumulation term will be ignored.

$$\text{Accumulation} = \text{Zero} \tag{5}$$

The overall mass balance for the sorbate in the gas phase of the unreacted shell then becomes:

$$\frac{\partial}{\partial r}\left(-4\pi r^2\, p\mathscr{D}_f \frac{\partial x}{\partial r}\right) \partial r = 0 \tag{6}$$

Since assumption 6 indicates $\mathscr{D}_f$ is independent of temperature, equation 6 can be integrated independently of a particle energy balance provided the boundary conditions are temperature independent. At the particle surface, the sorbate mole fraction must be the same as the bulk phase mole fraction. At the reaction interface, the sorbate mole fraction is zero due to the infinitely fast reaction. These two temperature independent boundary conditions are:

$$\text{Particle Exterior:} \quad r = a,\ x = X_G \tag{7}$$

$$\text{Reaction Interface:} \quad r = z,\ x = \text{Zero} \tag{8}$$

The solution of the mass balance equation (6), subject to boundary conditions (7) and (8), is

$$x = \frac{X_G\ a}{r} \cdot \frac{(r - z)}{(a - z)} \tag{9}$$

The rate at which the sorbate enters the particle by diffusion is:

$$+ 4\pi\, a^2\, p\, \mathscr{D}_{o} f_{o} \left(\frac{\partial x}{\partial r}\right)_a \tag{10}$$

APPENDIX A

or

$$\text{Input} = + \frac{4\pi\ a\ p\mathcal{D}_o f_o\ XG\ \ z}{a - z} \qquad (11)$$

based on equation (9).

The total amount of gas phase sorbate reacted or deposited on the particle at any time is:

$$\frac{4}{3}\ \pi\ Mo\ (a^3 - z^3) \qquad (12)$$

The rate at which this reaction occurs is:

$$\frac{\partial}{\partial t}\quad \left[\frac{4}{3}\ \pi\ Mo\ (a^3 - z^3)\right] \qquad (13)$$

which reduces to:

$$\text{Reacted} = \ - 4\pi\ Mo\ z^2\ \frac{\partial z}{\partial t} \qquad (14)$$

provided assumption (3) on temperature and concentration independence of sorbent saturation level Mo holds.

No sorbate leaves the particle, so:

$$\text{Output} = \text{Zero} \qquad (15)$$

The inventory change in porous space of the outer shell is again assumed negligible:

$$\text{Accumulation} = \text{Zero} \qquad (16)$$

The overall particle mass balance for the sorbate H_2S is obtained through substitution into equation (1):

APPENDIX A

$$+ 4\pi \frac{a\ p\ \mathscr{D}_o f_o\ X_G\ z}{a - z} = - 4\pi\ Mo\ z^2 \frac{\partial z}{\partial t} \tag{17}$$

or

$$\frac{a\ p\ \mathscr{D}_o f_o\ X_G\ z}{a - z} = - Mo\ z^2 \frac{\partial z}{\partial t} \tag{18}$$

It is convenient to express this equation in the following dimensionless terms:

Dimensionless Mole Fraction:

$$F = \frac{X_G}{X_G^o} \tag{19}$$

Dimensionless Radial Distance of Reaction Zone:

$$Z = \frac{z}{a} \tag{20}$$

Dimensionless Time:

$$\tau = \frac{X_G^o f_o\ V_o\ t}{(1-E)\ L\ M_o} \tag{21}$$

Dimensionless Adsorption (or Regeneration) Number:

$$- N_{Ad} = \frac{a^2 V_o}{(1-E)\ \mathscr{D}_o L P} \tag{22}$$

With the above substitution, equation (18) becomes:

$$- N_{Ad} \frac{\partial Z}{\partial \tau} = \frac{F}{Z\ (1 - Z)} \tag{23}$$

APPENDIX A

Equation (23) describes the unsteady state behavior of a single spherical particle in terms of two dimensionless groups, N_{Ad} and τ. τ or dimensionless time is also equal to the chemical efficiency of the bed at any time.

$$\tau = \frac{\text{Amount of Feed Gas Sorbate Processed}}{\text{Saturated Sorbent Bed Capacity}} \qquad (24)$$

VI. SORBENT BED MASS BALANCE

In the sorbent bed the mass balance for a gas phase sorbate are as follows:

$$\text{Input} = Vf\, X_G \qquad (25)$$

$$\text{Output} = Vf\, X_G + \frac{\partial}{\partial \ell}\,(Vf\, X_G)\, \partial \ell \qquad (26)$$

$$\text{Reacted} = gN\, \partial \ell \qquad (27)$$

$$\text{Accumulated} = E\, f\, \frac{\partial X_G}{\partial t}\, \partial \ell = \text{Zero} \qquad (28)$$

Substitution of the above into equation (1) leads to the overall sorbent bed mass balance:

$$-\frac{\partial}{\partial \ell}\,(Vf\, X_G) = gN \qquad (29)$$

The product Vf can be replaced by the constant $V_o f_o$ since the superficial velocity V is inversely proportional to gas density and the molar concentration f is directly proportional to gas density:

$$-V_o f_o\, \frac{\partial X_G}{\partial \ell} = gN \qquad (30)$$

The number of spherical particles per unit volume of bed is:

$$g = \frac{3\,(1 - E)}{4\pi\, a^3} \qquad (31)$$

The reaction rate per sphere is obtained from equations (14), (11), and (17).

$$N = \frac{4\pi\, a\, p \mathscr{O}_o f_o\, X_G\, z}{a - z} \tag{32}$$

The mass balance equation, (30), then becomes

$$- V_o f_o \frac{\partial X_G}{\partial \ell} = \frac{3\,(1 - E)\, p\, \mathscr{O}_o f_o\, X_G\, z}{a^2\,(a - z)} \tag{33}$$

With the previously defined dimensionless terms and

$$X = \frac{\ell}{L} \tag{34}$$

equation (33) becomes:

$$N_{Ad} \frac{\partial F}{\partial X} = - \frac{3\, FZ}{1 - Z} \tag{35}$$

Under the assumptions of the previous derivation and temperature independent boundary conditions, equations (23) and (35) may be solved independently of the sorbent bed energy balance equations that follow.

VII. PARTICLE ENERGY BALANCE EQUATION

Referring to Figure 1, the energy balance within a spherical particle at any radius r may be constructed as follows.

The overall energy balance must be satisfied.

Input = Output + Heat Consumed by Reaction + Heat Accumulated (36)

The rate at which heat enters a differential element of spherical sorbent particle is:

APPENDIX A

$$\text{Input} = -4\pi r^2 k_s \frac{\partial T_s}{\partial r} \tag{37}$$

The rate at which heat leaves the differential element is:

$$\text{Output} = -4\pi r^2 k_s \frac{\partial T}{\partial r} + \frac{\partial}{\partial r}\left(-4\pi r^2 k_s \frac{\partial T_s}{\partial r}\right) \partial r \tag{38}$$

Since the shrinking core model assumes reaction occurs only at $r = z$, the heat consumption term appears only in the boundary conditions and is zero elsewhere:

$$\text{Heat Consumed by Reaction} = \text{Zero} \tag{39}$$

Heat accumulated within a differential element is:

$$\text{Accumulated} = 4\pi r^2 \rho_s C_{ps} \frac{\partial T_s}{\partial t} \partial r \tag{40}$$

The overall energy balance for a spherical particle then becomes:

$$\frac{1}{r^2} \frac{\partial}{\partial r}\left(r^2 \frac{\partial T_s}{\partial r}\right) = \frac{\rho_s C_{ps}}{k_s} \frac{\partial T_s}{\partial t} \tag{41}$$

The boundary conditions of equation (41) are derived below.

At the particle surface, the heat flux into the particle is:

$$-4\pi a^2 k_s \left(\frac{\partial T_s}{\partial r}\right)_a \tag{42}$$

The heat flux at the particle surface may also be expressed in terms of the film heat transfer from the surrounding gas:

$$+4\pi a^2 h (T_G - T_S) \tag{43}$$

The boundary condition at the particle surface may thus be expressed by equating equations (42) and (43):

$$\text{at } r = a, -k_S \left(\frac{\partial T_S}{\partial r}\right)_a = h\,(T_G - T_S) \qquad (44)$$

At the reaction interface, the rate of heat consumption is:

$$\Delta H_R\, N \qquad (45)$$

The heat flux from the inner core to the reaction interface is:

$$-4\pi z^2 k_S \left(\frac{\partial T_S}{\partial r}\right)_{z-} \qquad (46)$$

The heat flux from the outer core to the reaction interface is:

$$4\pi z^2 k_S \left(\frac{\partial T_S}{\partial r}\right)_{z+} \qquad (47)$$

The boundary condition at the reaction interface thus involves a discontinuous first derivative obtained by equating heat fluxes to the interface (equations (46) and (47) to the heat consumption at the interface equation (45)).

$$\text{at } r = z,\ 4\pi z^2 k_S \left[\left(\frac{\partial T_S}{\partial r}\right)_{z+} + \left(\frac{\partial T_S}{\partial r}\right)_{z-}\right] = \Delta H_R\, N \qquad (48)$$

Substitution of the previously obtained value for N into equation (48) obtained for the bed mass balance (see equation 32) gives the boundary condition:

$$\text{at } r = z,\ \left(\frac{\partial T_S}{\partial r}\right)_{z+} = \left(\frac{\partial T_S}{\partial r}\right)_{z-} + \frac{\Delta H_R\, p \mathcal{O}_o f_o X_G\, a}{k_S\, z\,(a-z)} \qquad (49)$$

APPENDIX A

The boundary condition at the particle center is determined by setting the heat flux equal to zero:

$$\left(\frac{\partial T_S}{\partial r}\right)_0 = 0 \qquad (50)$$

At zero time, the sorbent particle is at its initial temperature:

$$\text{at} \quad t = 0 \quad T_S = T_O \qquad (51)$$

The particle energy balance and its boundary conditions can be expressed in dimensionless form using the previously defined dimensionless variables and the additional dimensionless variables:

Dimensionless Particle Temperature:

$$\Theta_S = \frac{T_S}{T_O} \qquad (52)$$

Dimensionless Gas Temperature:

$$\Theta_G = \frac{TG}{T_O} \qquad (53)$$

Dimensionless Radial Distance:

$$R = \frac{r}{a} \qquad (54)$$

Péclet Number Divided by Dimensionless Saturation Level:

$$N_{Pe} = \left(\frac{a^2 \rho_S Cp_S \; V_O}{L \; k_S}\right)\left(\frac{f_O \; XG_O}{M_O \; (1-E)}\right) \qquad (55)$$

APPENDIX A

Nusselt Number:

$$N_{Nu} = \frac{ha}{ks} \tag{56}$$

Dimensionless Heat of Reaction:

$$N_{Hr} = \frac{\Delta Hr \; p \mathcal{D}_o f_o \; X_{Go}}{T_o \; k_s} \tag{57}$$

With the indicated substitutions, the particle energy balance (41) and its boundary conditions (44), (49), (50), and (51) become:

$$\frac{1}{R^2} \frac{\partial}{\partial R} \left(R^2 \frac{\partial \Theta_s}{\partial R} \right) = N_{Pe} \frac{\partial \Theta_s}{\partial \tau} \tag{58}$$

at R = 1, $$- \left(\frac{\partial \Theta_s}{\partial R} \right)_{R = 1} = N_{Nu} \; (\Theta_G - \Theta_s) \tag{59}$$

at R = Z, $$\left(\frac{\partial \Theta_s}{\partial R} \right)_{Z+} = \left(\frac{\partial \Theta_s}{\partial R} \right)_{Z-} + N_{HR} \frac{F}{Z \; (1-Z)} \tag{60}$$

at R = 0, $$\left(\frac{\partial \Theta_s}{\partial R} \right)_0 = 0 \tag{61}$$

at $\tau = 0$, $$\Theta_s = 1 \tag{62}$$

VIII. BULK GAS PHASE ENERGY BALANCE EQUATION

The gas phase energy balance equation must satisfy the overall energy balance.

Input = Output + Heat Consumed by Reaction + Heat Accumulated (36)

APPENDIX A

The heat entering a differential cross section of bed is:

$$\text{Input} = V\rho_G\, C_{PG}\, T_G \tag{63}$$

The heat that leaves a differential element of bed is:

$$\text{Output} = V\rho_G\, C_{PG}\, T_G + \frac{\partial}{\partial \ell}\,(V\rho_G\, C_{PG}\, T_G)\;\partial\ell \tag{64}$$

The heat consumed within a differential cross section of bed is the heat that is transferred from the bulk gas phase of the bed to the sorbent particles:

$$\text{Heat Consumed by Reaction} = g\, 4\pi\, a^2\, h \left[T_G - (T_S)_a\right] \tag{65}$$

on, using the value for the number of particles per unit bed length obtained in equation (31):

$$\text{Heat Consumed} = \frac{3\,(1-E)\,h\,\left[T_G - (T_S)_a\right]}{a}\;\partial\ell \tag{66}$$

The heat accumulation of the gas is assumed to be negligible:

$$\text{Heat Accumulation} = \text{Zero} \tag{67}$$

The gas phase energy balance can now be constructed:

$$-\frac{\partial\,(V\rho_G\, C_{PG}\, T_G)}{\partial\ell} = \frac{3\,(1-E)\,h}{a}\left[T_G - (T_S)_a\right] \tag{68}$$

Since the gas velocity V is inversely proportional to gas density, the term $V\rho_G$ is constant:

$$V\rho_G = V_o\rho_{Go} \tag{69}$$

APPENDIX A

Using equation (69), the gas phase energy balance can be concisely expressed as:

$$+ \frac{\partial T_G}{\partial \ell} = - \frac{3\,(1 - E)\,h}{a\,C_{PG}\,V_o \rho_{Go}} \left[T_G - (T_S)_a \right] \tag{70}$$

With the additional dimensionless constant:

$$\text{Dimensionless Stanton Number} = N_{St} = \left(\frac{(1 - E)L}{a} \right) \left(\frac{h}{P_{GO}\,C_{PG}\,V_o} \right) \tag{71}$$

equation (70) becomes:

$$\frac{\partial \Theta_G}{\partial X} = - 3\,N_{St} \left[\Theta_G - (\Theta_S)_{R\,=\,1} \right] \tag{72}$$

IX. THE SORPTION DYNAMICS EQUATIONS WITH BOUNDARY CONDITIONS

The sorption dynamics equations derived in Sections V through VIII are listed in Table A2. The boundary equations are obtained from the following assumptions:

(1) At Initial time $\tau = 0$:

(1.a) The bed is unsaturated, $Z = 1$

(1.b) Bed temperature is at a constant initial value, $\Theta_G = \Theta_S = 1$

(1.c) No sorbate is in the gas phase of the bead, $F = 0$.

(2) At bed inlet conditions $X = 0$:

(2.a) The inlet gas is at a constant initial temperature, $\Theta_G = 1$

(2.b) The inlet gas contains a constant mole fraction of sorbate, $F = 1$

TABLE A2

THE SORPTION DYNAMICS

EQUATIONS WITH BOUNDARY CONDITIONS

1. THE PARTICLE MASS BALANCE

$$- N_{Ads} \frac{\partial Z}{\partial \tau} = Z \frac{F}{(1 - Z)}$$

B.C. at $\tau = 0$, $Z = 1$ and $F = 0$

2. THE BED MASS BALANCE

$$- N_{Ads} \frac{\partial F}{\partial X} = \frac{3 F Z}{1 - Z}$$

B.C. at $X = 0$, $F = 1$

3. THE PARTICLE ENERGY BALANCE

$$\frac{1}{R^2} \frac{\partial}{\partial R} \left(R^2 \frac{\partial \Theta_S}{\partial R} \right) = N_{Pe} \frac{\partial \Theta_S}{\partial \tau}$$

B.C. at $\tau = 0$, $\Theta_S = 1$ and $\Theta_G = 1$

at $R = 0$, $\frac{\partial \Theta_S}{\partial R} = 0$

at $R = Z$, $\left(\frac{\partial \Theta_S}{\partial R} \right)_{Z+} = \left(\frac{\partial \Theta_S}{\partial R} \right)_{Z-} + N_{H_R} \frac{F}{Z (1-Z)}$

at $R = 1$, $- \frac{\partial \Theta_S}{\partial R} = N_{Nu} (\Theta_G - \Theta_S)$

4. THE BULK GAS ENERGY BALANCE

$$\frac{\partial \Theta_G}{\partial X} = - 3 N_{st} \left[\Theta_G - (\Theta_S)_{R = 1} \right]$$

at $X = 0$, $\Theta_G = 1$

APPENDIX A

X. THE PARTICLE ENERGY BALANCE EQUATION FOR UNIFORM SORBENT PARTICLE TEMPERATURE

If heat transfer within a spherical sorbent particle becomes infinitely rapid, the particle temperature does not vary with radial distance. It may be demonstrated that the equations developed in Section VII show this behavior by increasing the particle conductivity to infinity and solving equations (58) through (62).

If k_s equals infinity, then:

$$N_{Pe} = N_{Nu} = N_{H_R} = 0 \tag{73}$$

$$\frac{1}{R^2} \frac{\partial}{\partial R} \left(R^2 \frac{\partial \Theta_s}{\partial R} \right) = 0 \tag{74}$$

$$\left(\frac{\partial \Theta_s}{\partial R} \right)_{R = 1} = 0 \tag{75}$$

$$\left(\frac{\partial \Theta_s}{\partial R} \right)_{Z+} = \left(\frac{\partial \Theta_s}{\partial R} \right)_{Z+} \tag{76}$$

$$\left(\frac{\partial \Theta_s}{\partial R} \right)_{R = 0} = 0 \tag{77}$$

The solution to equation (74) is:

$$R^2 \frac{\partial \Theta_s}{\partial R} = \text{Constant} \tag{78}$$

Boundary condition (75) can only be satisfied if Θ_s is constant.

Since the limiting solution to equations (58) through (62) yields no information on the dependence of particle temperature on time, the time dependence of particle temperature for the limiting case of infinite heat transfer within the particle is derived in this section.

The overall energy balance for a particle of uniform and time varying temperature is:

APPENDIX A

Heat Transferred to Particle = Heat Accumulated in Particle + Heat Consumed Within Particle (79)

The heat transferred from the bulk gas to the particle is determined by the film transfer coefficient and a temperature driving force:

$$\text{Heat Transferred to Particle} = 4\pi\, a^2\, h\, (T_G - T_S) \tag{80}$$

The heat accumulated within a spherical particle of uniform temperature is:

$$\text{Heat Accumulated Within Particle} = \frac{4}{3}\,\pi\, a^3\, \rho_S\, C\rho_S\, \frac{\partial T_S}{\partial t} \tag{81}$$

The heat consumed in the particle is:

$$\text{Heat Consumed Within Particle} = \Delta\, H_R\, N \tag{82}$$

The overall uniform particle energy balance can now be constructed.

$$4\pi\, a^2\, h\, (T_G - T_S) = \frac{4}{3}\,\pi\, a^3\, \rho_S\, C\rho_S\, \frac{\partial T_S}{\partial t} + \Delta\, H_R\, N \tag{83}$$

Substitution of the value for N derived for the bed mass balance (equation (32)) leads to the equation:

$$ah\, (T_G - T_S) = \frac{a^2\, \rho_S\, C_{PS}}{3}\, \frac{\partial T_S}{\partial t} + \frac{\Delta\, H_R\, p\mathscr{C}of_O\, X_G\, z}{a - z} \tag{84}$$

Equation (84) can be expressed in terms of the previously defined dimensionless variables:

$$N_{Nu}\, (\Theta_G - \Theta_S) = \frac{1}{3}\, N_{Pe}\, \frac{\partial \Theta_S}{\partial \tau} + N_{Hr}\, \frac{F\, Z}{(1 - Z)} \tag{85}$$

APPENDIX A

XI. THE ENERGY BALANCE EQUATIONS FOR EQUAL GAS AND PARTICLE TEMPERATURE

For the case where gas and particle temperature are equal the two energy balance equations reduce to one hyperbalic partial differential equation. This equation can be obtained by solving equations (85) and (72) simultaneously, then setting Θ_S equal to Θ_G:

$$\frac{\partial \Theta_G}{\partial X} = -3 N_{st} (\Theta_G - \Theta_s) \qquad (72)$$

$$\frac{1}{3} N_{Pe} \frac{\partial \Theta_s}{\partial \tau} + N_{Hr} \frac{F Z}{1 - Z} = N_{Nu} (\Theta_G - \Theta_s) \qquad (85)$$

$$-\frac{\partial \Theta_G}{\partial X} = \frac{N_{st} N_{Pe}}{N_{Nu}} \frac{\partial \Theta_s}{\partial \tau} + \frac{3 N_{HR} N_{st}}{N_{Nu}} \frac{FZ}{1-Z} \qquad (86)$$

$$\frac{\partial \Theta}{\partial X} + \frac{N_{st} N_{Pe}}{N_{Nu}} \frac{\partial \Theta}{\partial \tau} = -\frac{3 N_{HR} N_{st}}{N_{Nu}} \frac{FZ}{1-Z} \qquad (87)$$

APPENDIX B

DESCRIPTION OF THE ERDA PRESSURE UNIT

FROM SECTIONS 5.1 AND 5.2 OF FINAL REPORT, CONTRACT E(49-18)-1510

5.1 Description of Flows

The Linwood Pressure Unit (LPU) was placed in service the second week of September 1974. The flow scheme of the LPU is diagrammed in Figure 5.1 and outlined below.

1. The gases enter the system individually through a bank of rotameters and are mixed in situr during transport to the reactor, except for steam, which is pumped in separately joining the bulk of the flow at the bronze block process gas preheater. The gas supply is an external bank of cylinders of pure gas components. Steam supply is from a reservoir of deionized water.

2. CO passes through a separate preheater, the CO gas preheater, which is provided solely for heating the CO feed gas. The CO joins the other gases at the reactor inlet in order to eliminate coking in the main feed lines to permit long-term operation.

3. H_2S bypasses all preheaters and joins the other gases at the reactor inlet. This is to minimize exposure of metal to hot H_2S atmospheres.

FIGURE 5.1

SIMPLIFIED FLOW DIAGRAM FOR LINWOOD PRESSURE UNIT

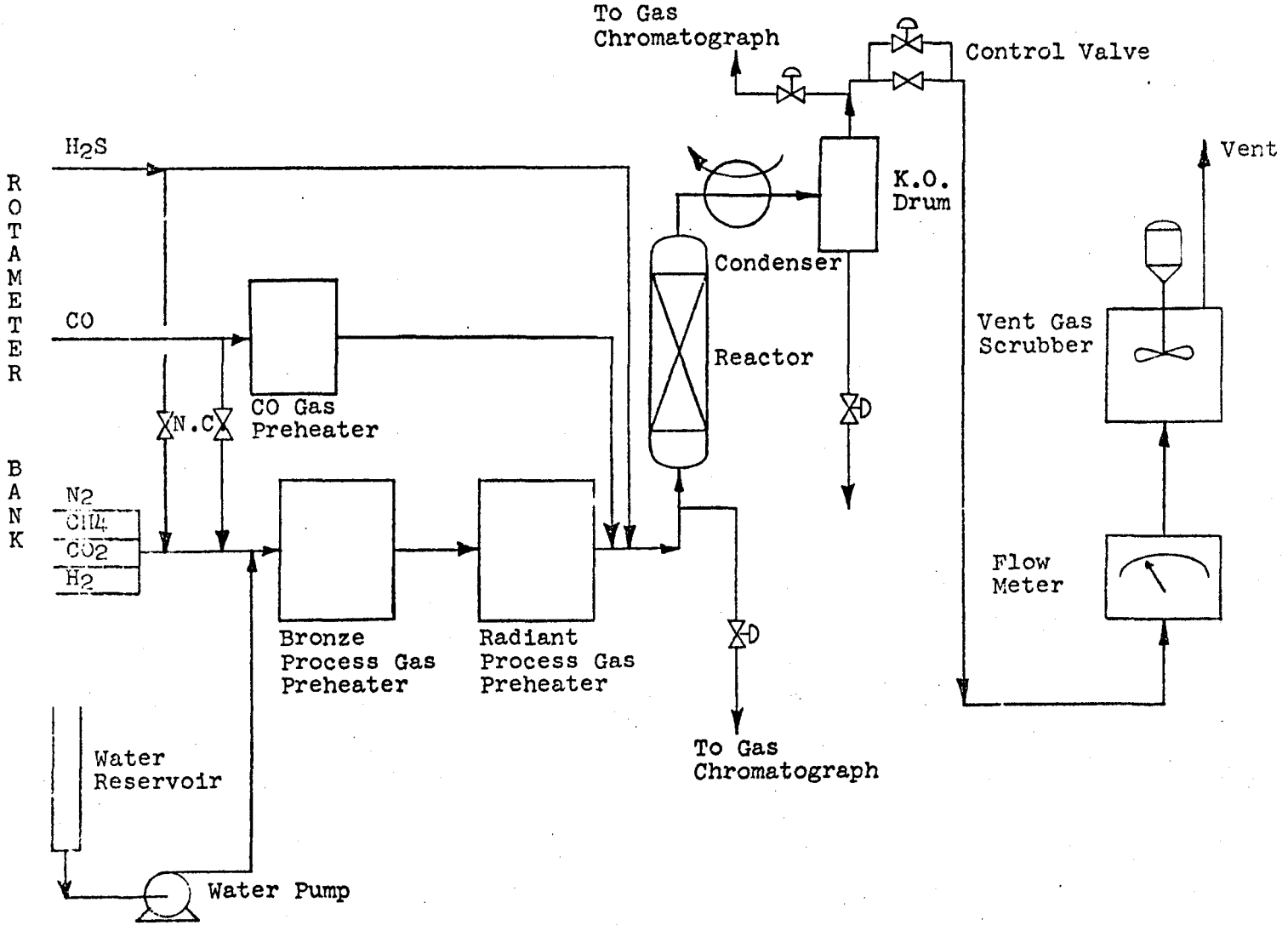

4. The other gases (N_2, CH_4, CO_2, H_2, steam) flow through the bronze block process gas preheater to the radiant process gas preheater, mix with the H_2S and CO flows, enter the reactor bottom and exit through the reactor top.

5. From the reactor, the gas stream is cooled to condense and remove moisture from the system.

6. After removing the water, the saturated gas stream flows through a pressure regulator, through a flow meter and out through the vent gas scrubber which consists of a solution of cupric nitrate and water. The scrubber acts as an environmental guard to prevent the venting of H_2S to the atmosphere.

7. Just before the gas stream passes through the pressure regulator, a side stream is removed and taken over to the automatic chromatograph. The chromatograph gives a continuous printout of the CO_2 and H_2S concentrations in the moisture-free effluent stream. This location for the side stream is to insure adequate pressure to permit consistent operation of the chromatograph.

A layout of the Linwood Pressure Unit showing the equipment arrangement is presented in Figure 5.2.

5.2 Description of Equipment

5.2.1 Piping - All piping that comes in contact with the hot gases is Inconel 601. This includes the pipe in the bronze process gas and radiant process gas pre-

FIGURE 5.2
LAYOUT OF LINWOOD PRESSURE UNIT

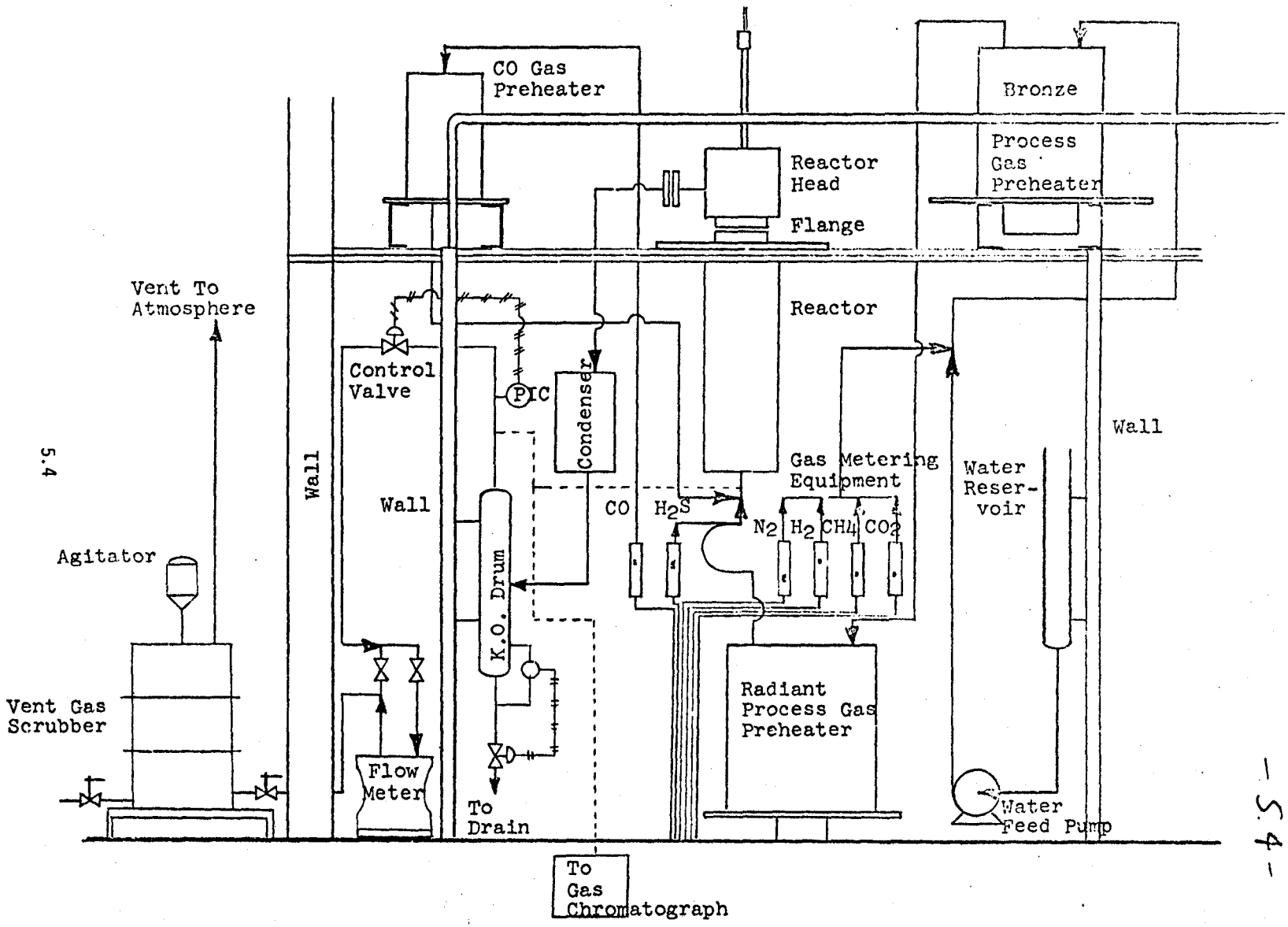

heaters, transfer lines between preheaters and between radiant preheater and reactor, and the reactor casing itself. Other metallic surfaces are either 316 S.S. or 304 S.S. including valves, transfer lines to and from rotameters, CO gas preheater lines and the stone loading basket. Inconel 601 was chosen after an investigation involving a search of the literature and discussions with various alloy companies in attempts to find a material that can withstand corrosive H_2S atmospheres at high temperatures and elevated pressures. Inconel 601 exhibited the best composite properties with respect to H_2S, steam, H_2, pressure and temperature.

5.2.2 Reactor and Stone Loading Basket - The reactor is a shell of Inconel 601, 5/8" thick, that houses the removable stone loading basket. The reactor consists of two parts, an upper reactor and a lower reactor, which are connected by a 3" flange. Figure 5.3 shows the assembled reactor and flange. This 3" flange is rated to 2500 psi and literally dwarfs the reactor itself. The top of the reactor acts as a collecting space for the gases after reaction. It contains a temperature radiation shield, a heating circuit to compensate for heat losses and the exit pipe for the gases. The top of the reactor is detailed in Figure 5.4. The lower reactor is a shell for the stone loading basket with a gas mixing space provided in the bottom.

FIGURE 5.3

INTERNAL THERMOCOUPLE ARRANGEMENT FOR ASSEMBLED REACTOR

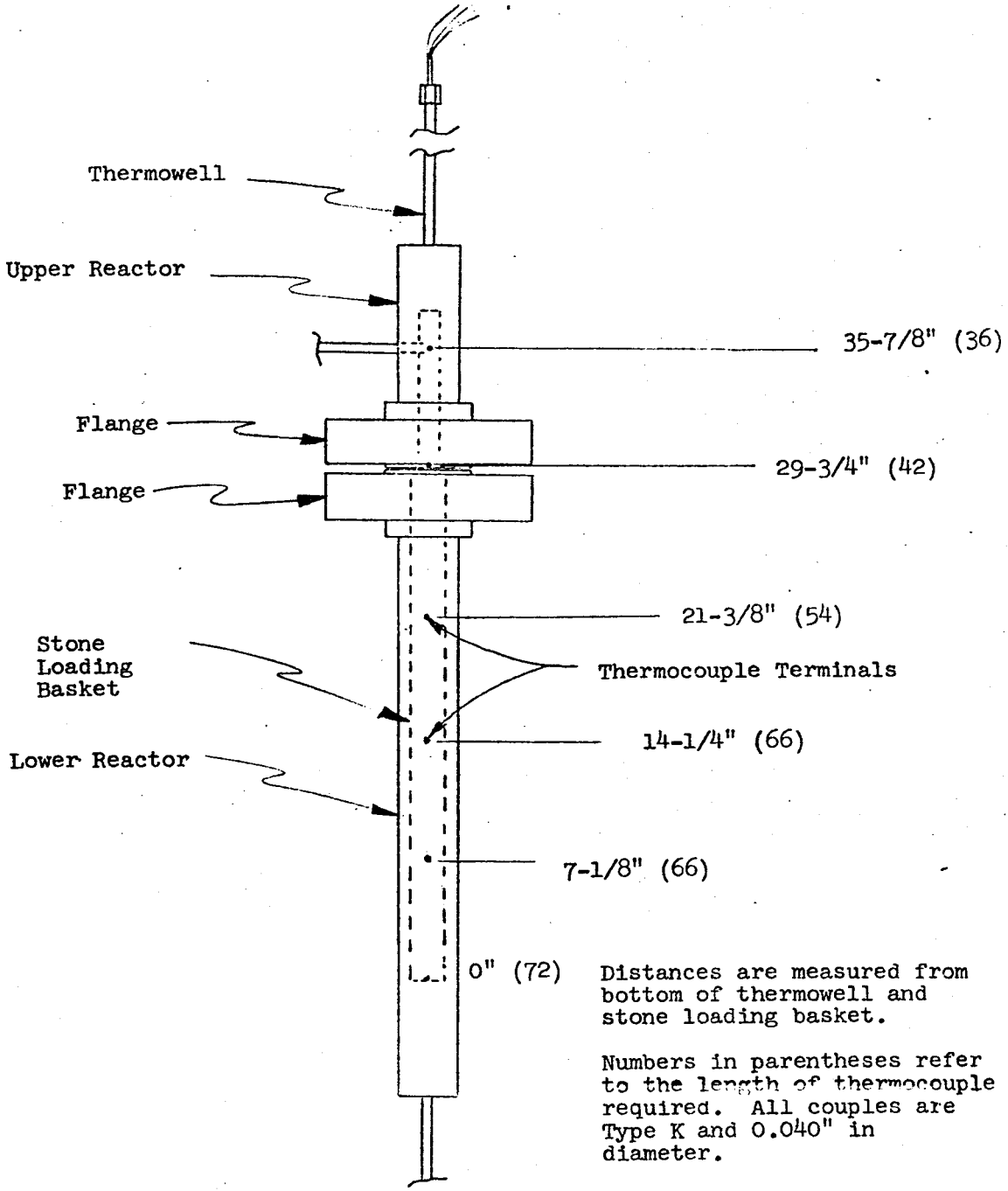

FIGURE 5.4

UPPER REACTOR ASSEMBLY

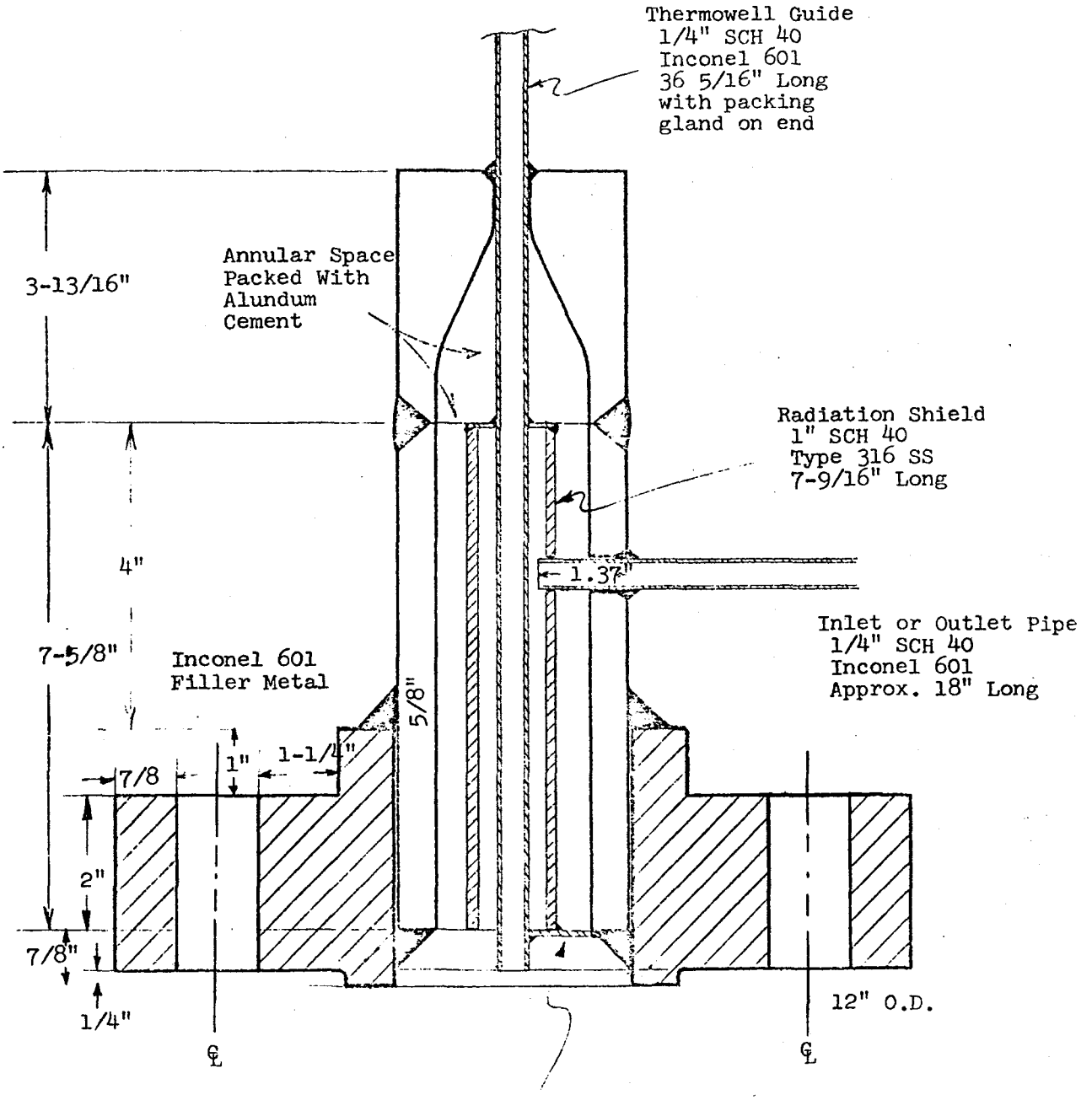

FIGURE 5.5
LOWER REACTOR ASSEMBLY
WITH FLANGE AND STONE LOADING BASKET

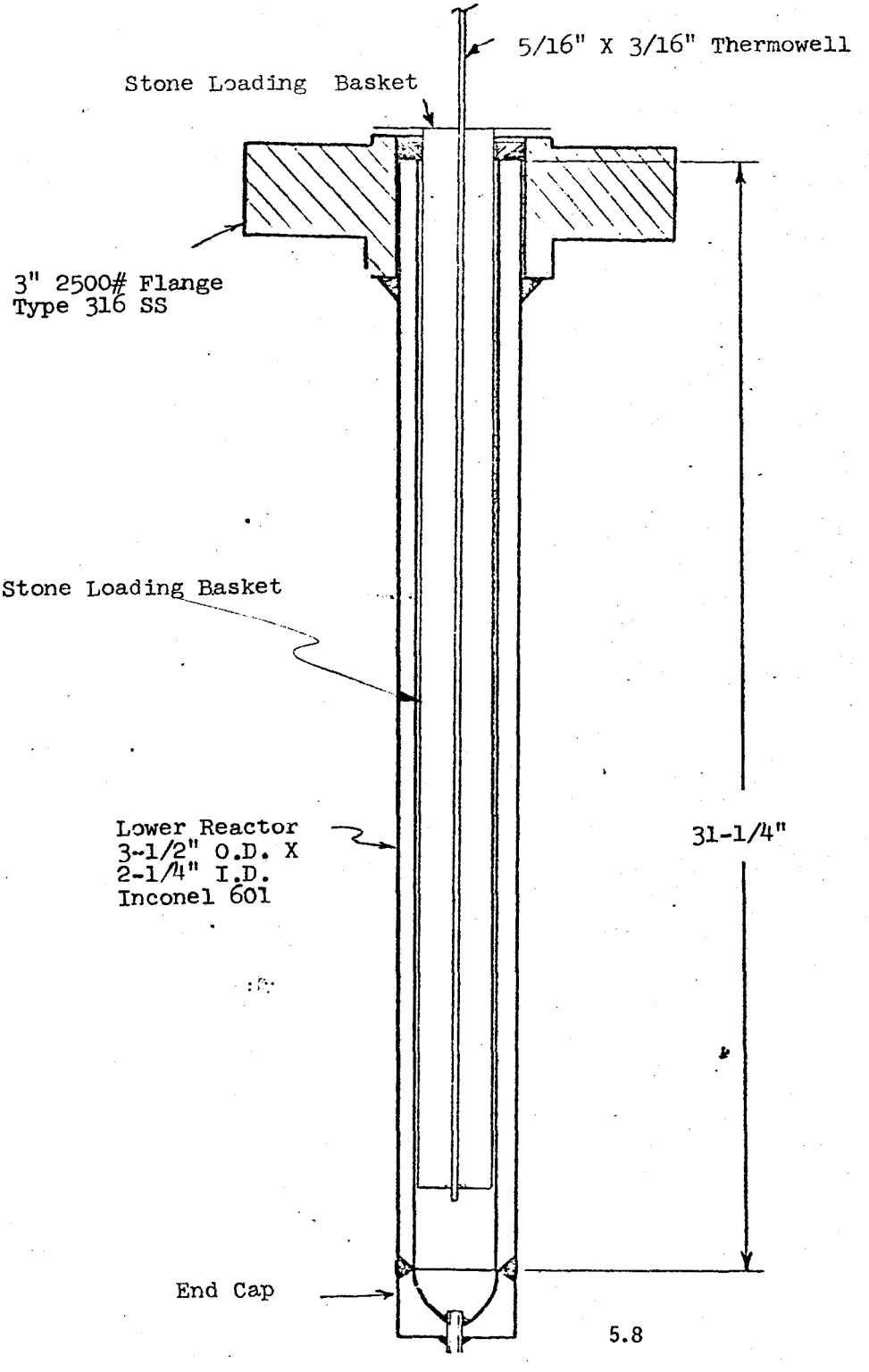

Figure 5.5 presents the lower reactor in detail. The reactor is equipped for adiabatic operation to prevent the loss of heat.

The adiabatic equipment consisted of a heating coil wrapped around the top of the reactor and three heating coils placed within the insulation around the lower reactor. The upper reactor heating coil is manually controlled by a Variac together with an "on-off" temperature controller. The lower reactor's three heating coils divide the lower reactor into three heating zones - top, middle and bottom. Each of these heating zones is controlled by an automatic differential temperature controller. The differential controller activates the heating element when there is a temperature difference between a thermocouple placed within the insulation near the reactor and a thermocouple placed within the insulation near the heating coil. Thus, it replaces any heat lost by balancing the temperatures at the two thermocouples. Figure 5.6 illustrates the location of the three heating zones within the insulation of the lower reactor. This sketch also shows the placement of the thermocouples that activate the differential controllers.

The basket fits inside the reactor with a 45/1000" tolerance. The basket is sized to hold 1 liter of limestone, and is made to be completely removable for

FIGURE 5.6
INSULATED REACTOR
SHOWING POSITIONS OF DIFFERENTIAL CONTROLLER THERMOCOUPLES

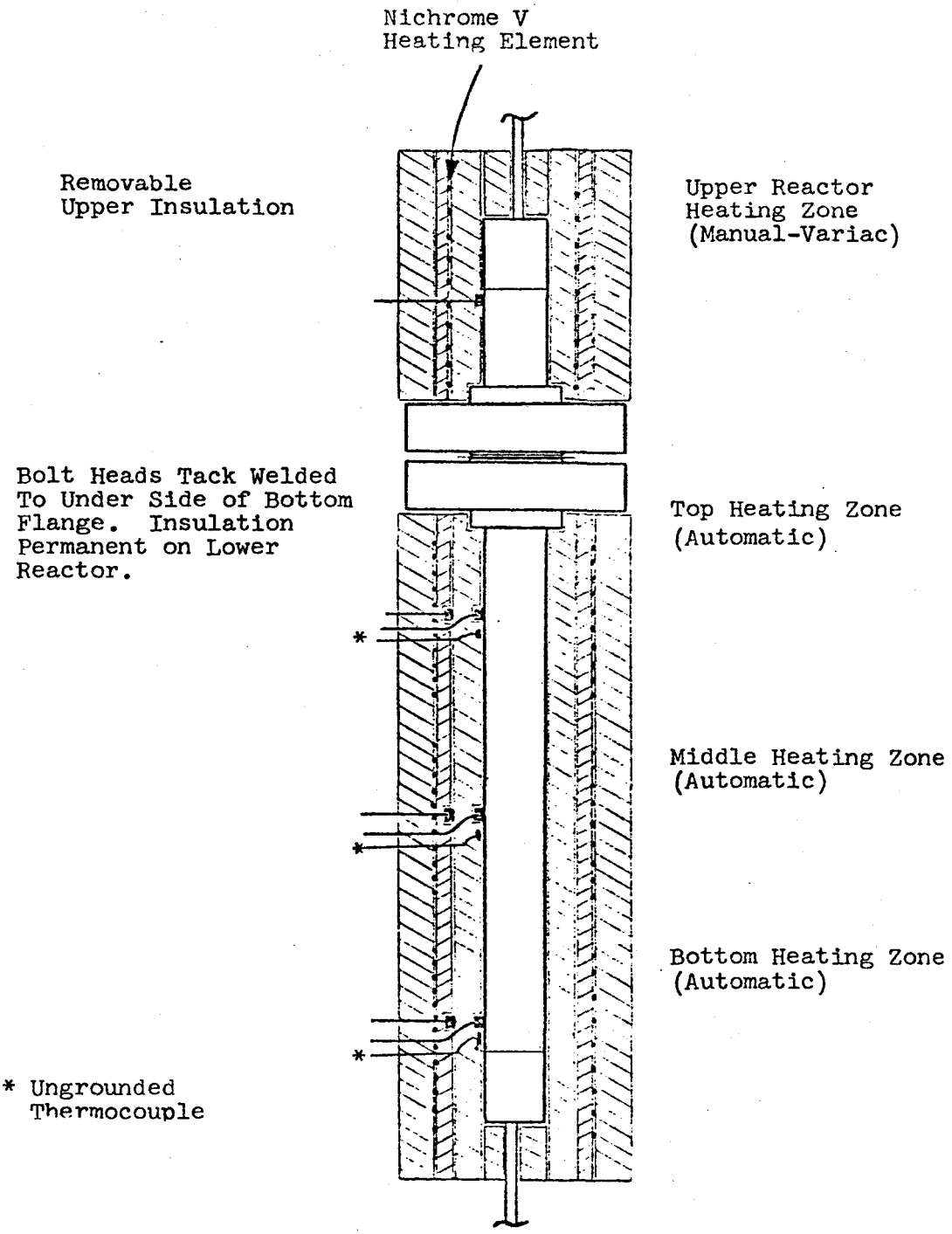

FIGURE 5.7

STONE LOADING BASKET SHOWING INTERNALS

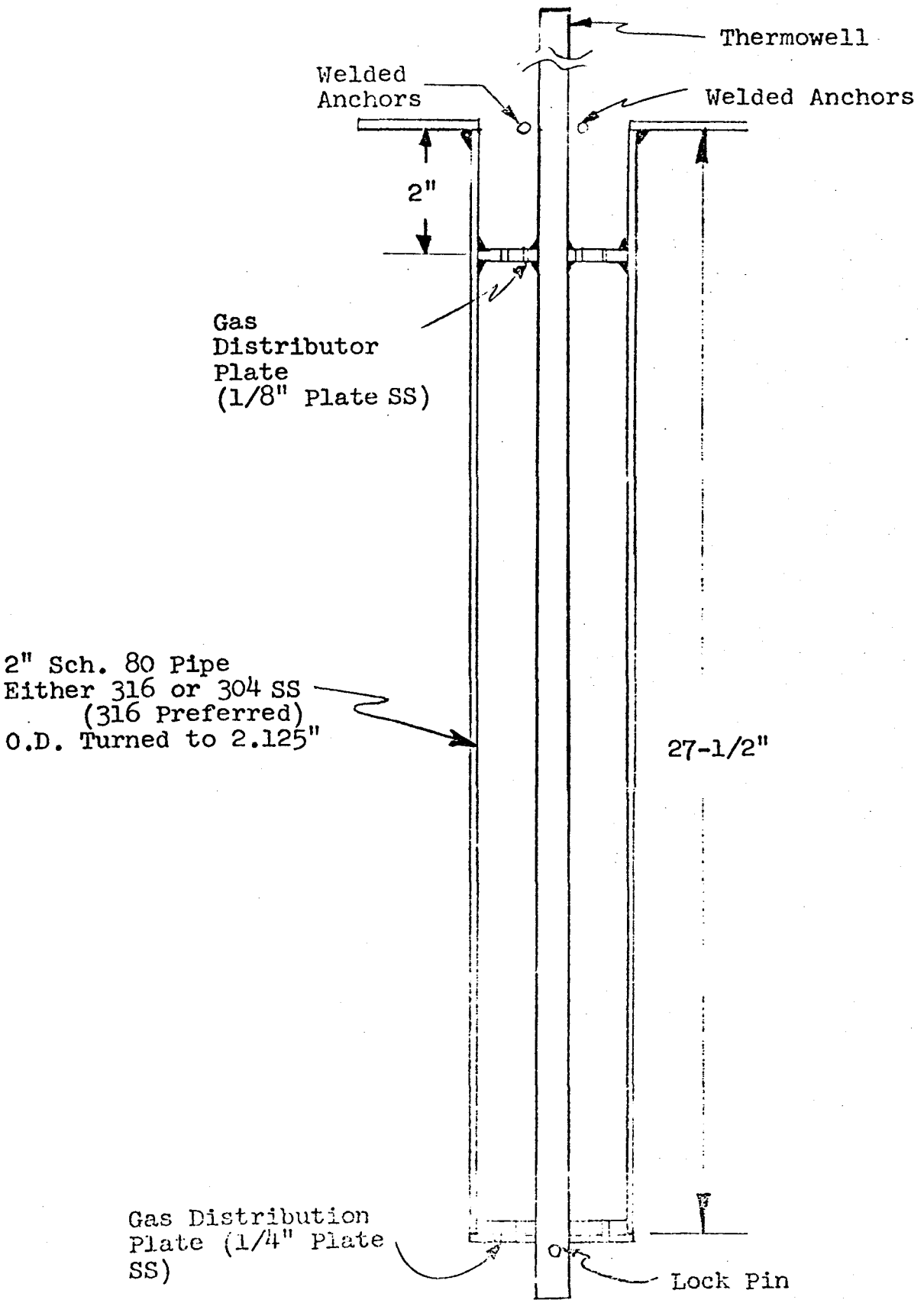

easy loading and unloading. A sketch of the stone loading basket appears as Figure 5.7. The basket has two welded anchors at the top to permit access for a hook connected to a hoist which is used to remove the basket from the reactor. The basket has one gas distribution plate at the bottom and one recessed two inches from the top to contain the limestone and permit an even gas stream flow through the bed. A concentric thermowell is secured to the top gas distribution plate and houses four thermocouples to enable recording of internal limestone bed temperatures.

The reactor and basket were originally designed to be down-flow through a fixed bed of limestone. This flow plan had to be revised when adiabatic operation of the unit proved to be unobtainable due to the large heat losses then being experienced from the flange. These heat losses came from the feed gas and affected the bed temperature. They occurred through the reactor flange which could not be insulated without affecting its strength characteristics and perhaps causing it to fail. Since adiabatic operation was necessary, the reactor was changed to an up-flow design so that the heat losses would come from the exit gases rather than the feed gases, enabling close to adiabatic operation within the bed. Heat losses from this exit stream had no significance. With up-flow operation the flange again turned out to be such a huge heat sink that the bed temperature

was adversely affected, making adiabatic operation impossible. The flange was insulated in spite of any effect that might occur on strength characteristics. Flange temperatures were monitored to prevent failure. The flange is shown in Figure 5.8 showing placement of basket, gaskets and flange.

5.2.3 Preheaters - There are three preheaters used in the process - CO gas, bronze block process gas and radiant process gas. All are electric powered. The CO gas and bronze block process gas preheaters are each bronze block preheaters that are made of coils of pipe with solid bronze cast around them. The heat is transmitted to the bronze by conduction through the ceramic heater coil sleeves to the bronze block. The radiant process gas preheater is comprised of coils of pipe with heating coils surrounding the pipe coils. Heat is transmitted by radiation to the pipe coils. The radiant process gas preheater was designed because the bronze process gas preheater could not heat the feed gases to required operating temperatures (see pre-startup problems).

5.2.4 Chromatograph - The chromatograph is an Applied Automation Model 102 with one sample loop for analysis of adsorption concentrations of CO_2 and H_2S and one sample loop for analysis of regeneration concentrations of CO_2 and H_2S. Samples are taken automatically every 5-1/2

FIGURE 5.8
FLANGE, BASKET, AND GASKETS ASSEMBLED

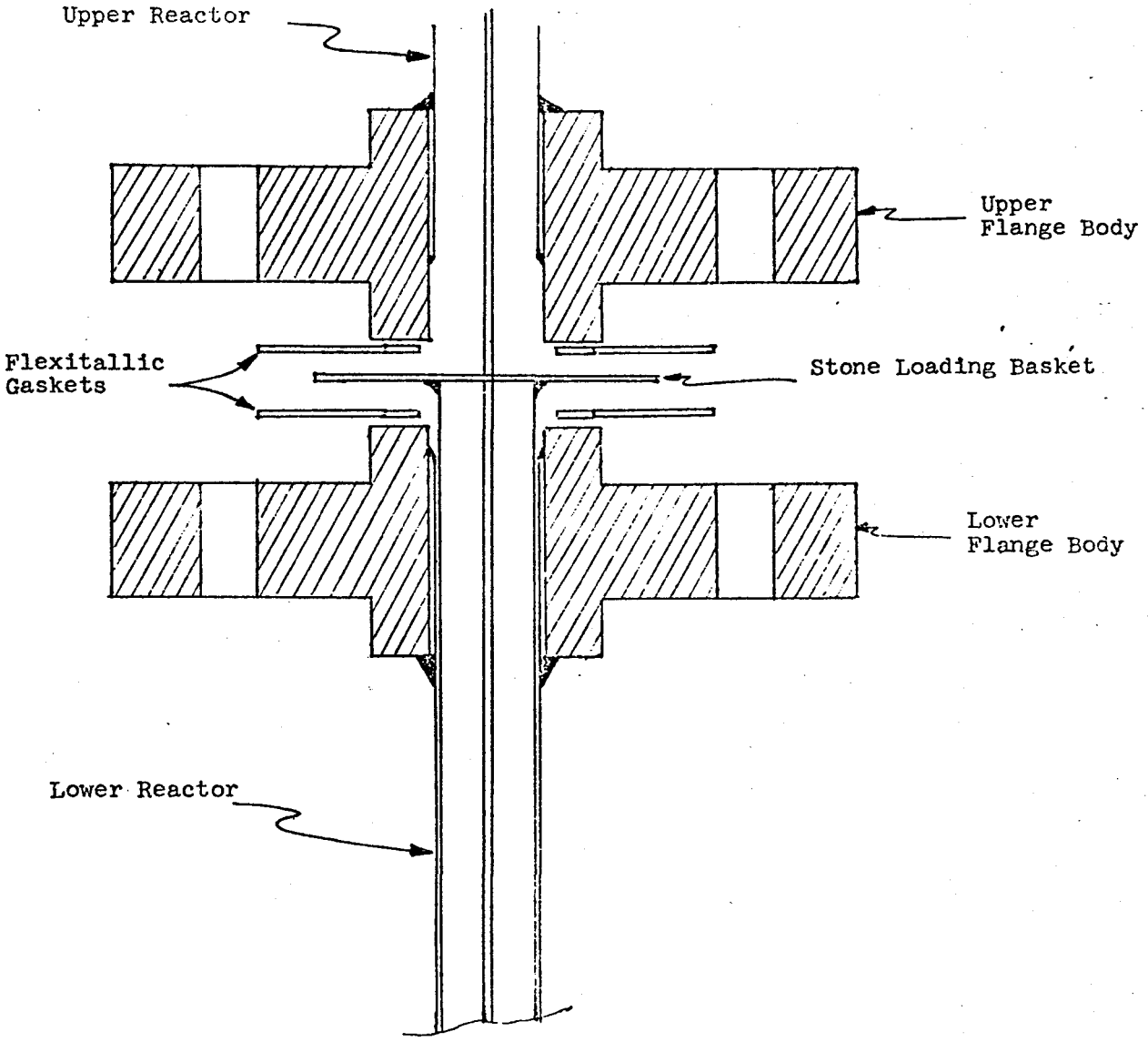

minutes and results are printed on a digital printer as well as a bar chart recorder. Some operating problems were encountered with the chromatograph which are discussed later in this report.

5.2.5 Vent Gas Scrubber - This scrubbing system consists of a 55-gallon drum with 50 gallons of 10% (wt) solution of cupric nitrate in water with an electric agitator on top. This system removes H_2S from process gases venting to the atmosphere. This is necessary for:

a. Adsorption effluents when limestone is no longer effective in removing H_2S;

b. Regeneration effluents when H_2S is being formed and removed from the limestone.

The gas enters through the bottom and as it flows through the solution; the stirrer keeps the two phases well mixed. This enables the H_2S to react with the cupric nitrate according to the chemical equation:

$$H_2S + Cu(NO_3)_2 \longrightarrow CuS + 2HNO_3$$